



Published in final edited form as:

Cell Metab. 2022 January 04; 34(1): 171–183.e6. doi:10.1016/j.cmet.2021.12.004.

## FGF1 and insulin control lipolysis by convergent pathways

Gencer Sancar<sup>1</sup>, Sihao Liu<sup>1</sup>, Emanuel Gasser<sup>1</sup>, Jacqueline G. Alvarez<sup>1</sup>, Christopher Moutos<sup>1</sup>, Kyeongkyu Kim<sup>1</sup>, Tim van Zutphen<sup>3</sup>, Yuhao Wang<sup>1</sup>, Timothy F. Huddy<sup>1</sup>, Brittany Ross<sup>1</sup>, Yang Dai<sup>1</sup>, David Zepeda<sup>1</sup>, Brett Collins<sup>1</sup>, Emma Tilley<sup>1</sup>, Matthew J. Kolar<sup>2</sup>, Ruth T. Yu<sup>1</sup>, Annette R. Atkins<sup>1</sup>, Theo H. van Dijk<sup>3</sup>, Alan Saghatelian<sup>2</sup>, Johan W. Jonker<sup>3</sup>, Michael Downes<sup>1,\*</sup>, Ronald M Evans<sup>1,4,\*</sup>

<sup>1</sup>Gene Expression Laboratory, Salk Institute for Biological Studies, La Jolla, California 92037, USA.

<sup>2</sup>Clayton Foundation Laboratories for Peptide Biology, Salk Institute for Biological Studies, 10010 North Torrey Pines Road, La Jolla, CA 92037, USA.

<sup>3</sup>Section of Molecular Metabolism and Nutrition, Department of Pediatrics, University of Groningen, University Medical Center Groningen, Hanzeplein 1, 9713 GZ, Groningen, The Netherlands.

<sup>4</sup>Lead contact

### Summary

Inexorable increases in insulin resistance, lipolysis and hepatic glucose production (HGP) are hallmarks of Type 2 diabetes. Previously, we showed that peripheral delivery of exogenous fibroblast growth factor 1 (FGF1) has robust anti-diabetic effects mediated by the adipose FGF receptor (FGFR) 1. However, its mechanism of action is not known. Here we report that FGF1 acutely lowers HGP by suppressing adipose lipolysis. On a molecular level FGF1 inhibits the cAMP-Protein kinase A axis by activating phosphodiesterase 4D (PDE4D), which separates it mechanistically from the inhibitory actions of insulin on PDE3B. We identify Ser44 as an FGF1-induced regulatory phosphorylation site in PDE4D that is modulated by the feed-fast cycle. These findings establish the FGF1/PDE4 pathway as an alternate regulator of the adipose-HGP axis, and identify FGF1 as an unrecognized regulator of fatty acid homeostasis.

### Graphical Abstract

\*Correspondence: evans@salk.edu, downes@salk.edu.

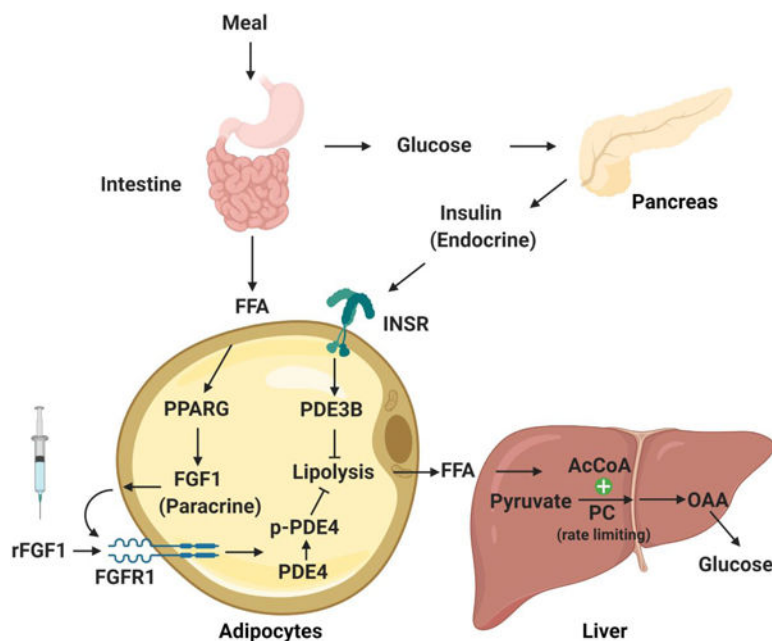
#### Author Contributions

G.S., M.D. and R.M.E designed the research, and G.S. performed most of the experiments. S.L. designed and performed *in vivo* (adR1KO) / *ex vivo* lipolysis (F1KO), pyruvate carboxylase activity assay, metabolite measurement (adR1KO) and ATGL inhibitor experiments. E.G. performed AAV injections. C.M. performed adipose transplantation studies. G.S., M.J.K and A.S performed the metabolite profiling *via* mass-spectrometry. J.G.A., T.F.H., Y.D., Y.W., B.R., D.Z., B.C., K.K., and E.T. performed research. T.H.v.D. and J.W.J. performed clamp studies. T.v.Z performed  $\beta$ -oxidation assay. G.S., A.R.A, R.T.Y, M.D, and R.M.E analyzed the data and prepared the manuscript.

**Publisher's Disclaimer:** This is a PDF file of an unedited manuscript that has been accepted for publication. As a service to our customers we are providing this early version of the manuscript. The manuscript will undergo copyediting, typesetting, and review of the resulting proof before it is published in its final form. Please note that during the production process errors may be discovered which could affect the content, and all legal disclaimers that apply to the journal pertain.

#### Declaration of interests

A.R.A., R.T.Y., M.D., and R.M.E are co-inventors of mutated FGF1 proteins and methods of use and maybe entitled to royalties.



## eTOC blurb

Sancar et al. demonstrate that FGF1 acutely lowers hepatic glucose production by suppressing adipose lipolysis. While insulin suppresses lipolysis *via* adipose PDE3B, FGF1 is dependent on PDE4D allowing FGF1/PDE4D pathway to remain functional under insulin resistance. This paracrine FGF1/PDE4D pathway is responsive to feeding in the adipose tissue.

## Keywords

Type-2 diabetes; FGF1; lipolysis; cAMP; PDE4; hepatic glucose production

## Introduction

Chronic hyperglycemia and dyslipidemia are hallmarks of Type 2 diabetes mellitus (T2DM) attributed to the failure of insulin to appropriately suppress hepatic glucose production and adipose lipolysis. Moreover, unregulated lipolysis leads to the aberrant accumulation of free fatty acids (FFAs) in peripheral metabolic tissues including liver, muscle, and pancreatic islets, further exacerbating disease severity (Saponaro et al., 2015; Sears and Perry, 2015). Physiologically, adipose lipolysis is regulated, in part, by opposing hormonal stimuli that control cAMP levels and Protein kinase A (PKA) activity (Bartness et al., 2014; Duncan et al., 2007). Pro-lipolytic hormones (e.g. glucagon, growth hormone, thyroid hormone, cortisol, catecholamines) elevate cellular cAMP levels to drive PKA phosphorylation of key lipolytic proteins including perilipin and hormone-sensitive lipase (HSL). Conversely, insulin discovered 100 years ago remains the only known anti-lipolytic hormone, acting via phosphodiesterase 3B (PDE3B) to suppress cAMP levels and inhibit PKA activity (Kitamura et al., 1999; Strålfors and Honnor, 1989; Young et al., 2006). Phosphodiesterases (PDEs) catalyze the conversion of cAMP to AMP. To date, 11 PDE families (PDE1-PDE11)

each encompassing multiple isoforms have been described (Azevedo et al., 2014). In adipose tissue in particular, different PDE4 isoforms have been implicated in the regulation of the cAMP/PKA pathway, however their contributions to lipolysis are not known (Baeza-Raja et al., 2016; Grønning et al., 2006; Zhang et al., 2009). Notably, half of the PDE activity in adipocytes is attributed to PDE4A-D, where the isoform-specific N-terminal domains regulate protein-protein interactions and subcellular localizations (Houslay and Adams, 2003; Young *et al.*, 2006). Consistent with this, PDE4 inhibitors enhance lipolysis, particularly when PDE3 activity is inhibited (Dipilato et al., 2015; Grønning *et al.*, 2006; Kraynik et al., 2013; Snyder et al., 2005). Mice deficient in PDE4A, PDE4B and PDE4D genes were previously generated (Jin and Conti, 2002; Jin et al., 2005; Jin et al., 1999). Loss of PDE4A and PDE4B in adipocytes led to increased cAMP levels without affecting lipolysis (Grønning *et al.*, 2006; Zhang *et al.*, 2009). In contrast, adipocyte PDE4D expression is induced by insulin and synthetic catecholamines, and lower PDE4D levels are associated with increased  $\beta$ -adrenergic signaling, implicating a potential role in lipolysis (Jang et al., 2020; Oknianska et al., 2007).

Fibroblast growth factor 1 (FGF1) has an established role in adaptive adipose remodeling (Jonker et al., 2012; Wang et al., 2020). Mice lacking FGF1 develop a more aggressive diabetic phenotype in response to a dietary challenge (high fat diet, HFD) that is, in part, attributed to a failure to appropriately remodel adipose tissue. FGF1 expression in adipose tissue is controlled by PPAR $\gamma$  and is robustly induced in the fed state and upon HFD feeding (Choi et al., 2016; Jonker *et al.*, 2012). In addition, peripheral delivery of FGF1 rapidly lowers blood glucose levels in diabetic mouse models in an adipose FGF receptor (FGFR) 1-dependent manner, however the underlying mechanism(s) is not understood (Suh et al., 2014). Here we show that FGF1 suppresses adipose lipolysis and demonstrate that the anti-lipolytic activities of FGF1 are required for acute glucose lowering. On a molecular level, we discovered that these actions are mediated by the activation of PDE4D in adipose tissue.

## Results

### FGF1 suppresses adipose lipolysis in an adipose FGFR1-dependent fashion

To validate that FGF1-induced glucose lowering is dependent on FGFR1 expression in adipose tissue, FGFR1 was selectively deleted in mature adipocytes (*Fgfr1* fl/fl crossed to adiponectin-CRE, adR1KO mice). FGF1 rapidly decreased blood glucose levels in diet-induced obese (DIO) wild type mice (0.5 mg/kg FGF1 s.c., adR1WT) but failed to affect adR1KO mice, consistent with our previous findings (Suh *et al.*, 2014) (Figure S1A). Given the increase in insulin levels in adR1KO mice (Table S1), and the link between hepatic glucose production (HGP) and lipolysis, we hypothesized that FGF1 may affect adipose lipolysis (Perry et al., 2015a; Perry et al., 2018; Rebrin et al., 1996). To explore this notion, we initially determined whether lipolysis was perturbed in FGF1 knockout (F1KO) mice. While no differences were seen in serum FFA levels in fed mice, the higher serum insulin levels in F1KO mice suggested a dysregulated lipolytic response compensated by insulin (Figure S1B). Indeed, *ex vivo* lipolysis assays in the absence of insulin compensation revealed markedly elevated lipolysis in the gonadal adipose tissue (gWAT) of F1KO mice

(Figure 1A). The persistence of the increased *ex vivo* lipolysis in F1KO gWAT in an adipose transplant model was indicative of an adipose-autonomous effect (Figure S1C and D). Supporting this notion, mice harboring the selective deletion of FGF1 in adipose tissue (*Fgf1* fl/fl crossed to adiponectin Cre) showed a similar increase in gWAT *ex vivo* lipolysis (Figure S1E). In addition, FGF1 acutely suppressed basal and isoproterenol-induced lipolysis in mouse and human stromal vascular fraction (SVF)-derived adipocytes, consistent with an adipocyte-intrinsic effect (Figure 1B and Figure S1F). Similarly, FGF1 dose-dependently suppressed isoproterenol-induced lipolysis in 3T3-L1 adipocytes (Figure 1C), an effect that was blocked by FGFR1 inhibition (Figure S1G).

To determine whether exogenous FGF1 can similarly affect adipose lipolysis *in vivo*, DIO adR1WT and adR1KO mice were fasted overnight to minimize compensatory changes in insulin prior to injection with FGF1 (0.5 mg/kg s.c.). FGF1 reduced serum FFA levels in adR1WT mice by ~30%, but failed to affect adR1KO mice (Figure 1D). Moreover, *ex vivo* lipolysis was suppressed by FGF1 in an adipose FGFR1-dependent manner (Figure 1E and Figure S1H). As a measure of *in vivo* lipolysis, adR1WT and adR1KO mice pretreated with and without FGF1 were portally-infused with radiolabeled oleic acid. The fractional turnover rate of oleic acid was reduced in FGF1-treated adR1WT mice, indicative of lower basal lipolysis. In contrast, oleic acid turnover in adR1KO mice was not affected by FGF1 pretreatment (Figure 1F).

The above findings implicate FGF1-FGFR1 signaling as a novel pathway regulating adipose lipolysis. Of note, this regulation appears specific to white adipose depots, as FGF1 did not affect lipolysis in brown adipose tissue (Figure S1I). Moreover, FGF1 did not alter whole body metabolism, or affect circulating levels of leptin (Figure S1J, Table S1). To determine the contribution of lipolytic regulation to FGF1-mediated glucose lowering, lipolysis was pharmacologically blocked with atglistatin, an inhibitor of adipose triglyceride lipase (ATGL). Atglistatin (120 mg/kg p.o) rapidly lowered blood glucose levels in *ad lib* fed *ob/ob* mice, consistent with the indirect regulation of hepatic glucose production by the products of lipolysis (Perry *et al.*, 2015a). While as a single agent, FGF1 (0.5 mg/kg s.c.) robustly lowered blood glucose, no additive effects were seen when FGF1 was co-administered with atglistatin, supporting the notion that exogenous FGF1 lowers blood glucose by suppressing lipolysis (Figure 1G).

The rapid *in vivo* kinetics suggested that FGF1 may regulate lipolysis posttranslationally. To explore this possibility, we determined the ability of FGF1 to affect PKA-mediated activation of HSL. In 3T3-L1 adipocytes, FGF1 suppressed HSL phosphorylation at S<sup>660</sup> (pHSL) under both basal and isoproterenol (ISO)-stimulated conditions (Figure 1H and Figure S1K). Similarly, pHSL levels in gWAT were decreased 30 min after FGF1 injection (Figure 1I). Moreover, the *in vivo* suppression of HSL phosphorylation upon FGF1 treatment correlated with the *in vitro* suppression of lipolysis (Figure S1L).

### **FGF1 regulates hepatic glucose production (HGP)**

Insulin regulates blood glucose levels in part by suppressing lipolysis and thereby HGP, and dysregulated HGP contributes to hyperglycemia in insulin resistance (Boden *et al.*, 2017; Lin and Accili, 2011; Lombardo and Menahan, 1979; Turner *et al.*, 2005). To

determine whether the suppression of lipolysis by FGF1 acutely reduced HGP, we measured the ability of FGF1 to affect gluconeogenic substrate utilization. Notably, *ob/ob* mice pretreated with FGF1 had a markedly reduced ability to synthesize glucose from pyruvate (pyruvate tolerance test; PTT), while no differences were seen when glycerol was the exogenous substrate (glycerol tolerance test; Glycerol TT) (Figure 2A). These findings were replicated in DIO mice (Figure S2A). Moreover, the ability of FGF1 to suppress pyruvate utilization was dependent on adipocyte FGFR1 expression (Figure 2B). This differential sensitivity of pyruvate and glycerol utilization localized the effect of FGF1 on gluconeogenesis to a step downstream of pyruvate (Exton and Park, 1967; Shrago and Lardy, 1966) (Figure S2B). To further delineate the FGF1-sensitive step, the levels of gluconeogenic intermediates were measured by mass spectrometry in the livers of *ob/ob* mice 2 h after FGF1 injection. Intermediates downstream of pyruvate including glucose 6-phosphate (G6P), fructose 6-phosphate (F6P), phosphoglycerate (PG), phosphoenolpyruvate (PEP), and oxaloacetate (OAA) were reduced in FGF1 injected mice, whereas metabolites involved in the tricarboxylic acid cycle (TCA) cycle were not affected (Figure 2C and Figure S2C). Notably, these reductions in substrate levels occurred in the absence of changes in protein expression in the rate-limiting enzymes involved in gluconeogenesis (Figure S2D). In addition, levels of the allosteric activator of pyruvate carboxylase, acetyl-CoA were decreased (Figure 2C). These reductions in gluconeogenic substrates were largely recapitulated in adR1WT mice, whereas adR1KO mice were insensitive to FGF1 treatment (Figure 2D). Furthermore, an adipose FGFR1-dependent reduction in acetyl-CoA was accompanied by ~50% reduction in pyruvate carboxylase activity (Figure 2E). Acetyl-CoA is the product of fatty acid  $\beta$ -oxidation, hence the absence of any change in hepatic  $\beta$ -oxidation (Figure S2E) supports a mechanism in which the reduction of free fatty acids upon FGF1 treatment decreases the activity of pyruvate carboxylase and thereby, limits HGP.

To test the relevance of these findings to glucose homeostasis, a hyperinsulinemic clamp was performed on *ob/ob* mice after short-term serial FGF1 administration (0.5 mg/kg every other day for a week). This limited treatment regimen resulted in a ~25% reduction in basal endogenous glucose production (EGP) (Figure 2F). Under clamp conditions, a higher exogenous glucose infusion rate (GIR) was required to maintain the glucose set-point in FGF1-treated mice; an effect largely attributed to diminished EGP as the glucose disposal rate (GDR) was not altered (Figure 2F).

### FGF1 activation of PDE4 inhibits cAMP-PKA pathway

Insulin suppresses lipolysis via the PI3K-dependent activation of PDE3B (DiPilato et al., 2015a; Rahn et al., 1994). As FGFR1 activation can also signal via the PI3K pathway, we investigated whether the anti-lipolytic effects of FGF1 were affected by the PI3K inhibitor wortmannin. Paralleling insulin signaling, wortmannin abrogated the FGF1-induced reduction in FFA release in 3T3-L1 adipocytes (Figure S3A). In addition, FGF1 attenuated isoproterenol-induced increases in cAMP and cAMP/PKA signaling in a CRE-luciferase-based reporter system, implicating a possible effect on phosphodiesterase activity (Figure 3A and Figure S3B). Interestingly, inhibition of PDE3B did not impair FGF1-induced suppression of lipolysis (Figure S3C). In contrast, the anti-lipolytic activity of FGF1 was blocked by selective inhibitors of PDE4 in 3T3-L1 adipocytes, as well as in

mouse and human SVF-derived adipocytes (Figure 3B and S3D, S3E). Moreover, the FGF1-induced attenuation of an isoproterenol-driven increase in cAMP was lost in the presence of a PDE4 inhibitor, as measured in live 3T3-L1 cells using a fluorescence-based cAMP Biosensor (Tewson et al., 2016) (Figure 3C). No FGF1 effects were seen in cells expressing the GFP control (Figure S3F). To determine whether PDE4 activity was required for FGF1-induced suppression of lipolysis *in vivo*, DIO mice were gavaged with a PDE4 inhibitor 1 h prior to FGF1 injection. Analyses of adipose explants from those mice demonstrated that PDE4 inhibition blocked the ability of FGF1 to suppress lipolysis (Figure 3D, Figure S3G).

Given the above findings, we posited that FGF1-PDE4 signaling regulated HSL phosphorylation. Indeed, in both basal and isoproterenol-stimulated cells, the ability of FGF1 to suppress HSL phosphorylation was lost in the presence of the PDE4 inhibitor roflumilast (Figure S3H). The translocation of phosphorylated HSL to the lipid droplet and its subsequent interaction with perilipin is a key regulatory step in lipolysis (Clifford et al., 2000; Egan et al., 1992; Greenberg et al., 1991; Shen et al., 2009). To monitor the ability of FGF1 to affect pHSL-perilipin interactions in live cells, adeno-associated virus (AAV) vectors incorporating the human adiponectin promoter/enhancer to restricted expression to mature adipocytes (adAAVs) were used to express GFP-tagged perilipin (perilipin-GFP) and mCherry-tagged HSL (HSL-mCherry) in 3T3-L1 adipocytes (O'Neill et al., 2014). Importantly, FGF1 reduced the isoproterenol-induced co-localization of perilipin-GFP and HSL-mCherry, as seen in the temporal monitoring of fluorescence overlap and by confocal microscopy (Figures 3E left panel and S3I). No effects were seen in cells expressing perilipin-GFP and mCherry without the HSL fusion (Figure S3J). Moreover, while selective inhibition of PDE4 or PDE3 increased perilipin-HSL co-localization, consistent with increased cAMP levels and PKA activation, only PDE4 inhibition abrogated the FGF1 effect (Figure 3E, middle and right panels).

In combination, these findings suggested a model in which FGF1-FGFR1 activation of PDE4 attenuates cAMP/PKA phosphorylation of HSL and its subsequent association with perilipin on the lipid droplet surface. Based on previous studies linking PDE4D with adipose lipolysis, we explored whether overexpression of PDE4D is sufficient to recapitulate the ability of FGF1 to suppress lipolysis (Jang et al., 2019). Indeed, overexpression of 3 PDE4D isoforms dose-dependently suppressed lipolysis in 3T3-L1 adipocytes, with the PDE4D3 isoform showing the highest efficacy (Figure S3K). In order to extend on this finding, an adAAV vector was constructed that restricted PDE4D3 expression to mature adipocytes (O'Neill *et al.*, 2014) (Figures S3L–N). Notably, adAAV-PDE4D3-driven expression robustly suppressed isoproterenol-induced increases in lipolysis, cAMP, and perilipin-GFP/HSL-mCherry co-localization in 3T3-L1 adipocytes (Figure 3F–H). In addition, lower pHSL levels were seen in 3T3-L1 adipocytes infected with adAAV-PDE4D3 compared to control adAAV-GFP (Figure S3O). Furthermore, the reductions in isoproterenol-induced lipolysis and HSL phosphorylation with adAAV-PDE4D3 infection were conserved in human SVF-derived adipocytes (Figures S3P, Q).

### FGF1-induced glucose lowering is dependent on PDE4 *in vivo*

The finding that FGF1-induced suppression of lipolysis is dependent on PDE4 raised the possibility that this pathway contributes to glucose homeostasis in insulin-resistant mice. To explore this notion, *ad lib* fed DIO mice were treated with the PDE4 inhibitor roflumilast. In these mice, PDE4 inhibition transiently increased blood glucose, serum FFA and insulin levels (Figure 4A and B, Figure S4C). In fasted DIO mice, PDE4 inhibition led to a more sustained increase in blood glucose levels, presumably due to lower insulin levels and higher lipolysis in the fasted state (Figure S4A–C). Notably, the ability of FGF1 to reduce blood glucose levels was lost with roflumilast pretreatment of *ad lib* fed mice (Figure 4C). In contrast, inhibition of PDE3 failed to affect the ability of FGF1 to modulate glucose levels (Figure S4D). These data support a requirement for PDE4-dependent regulation of lipolysis in the glucose lowering effects of FGF1. Given the ability of PDE4D to regulate lipolysis *in vivo*, we explored the role of this PDE family in the metabolic actions of FGF1. Encouragingly, adipose explants from PDE4D KO mice showed higher basal and isoproterenol-stimulated lipolysis, and adipocytes derived from PDE4D KO SVF were insensitive to FGF1 treatment (Figure 4D, E). In addition, despite lower body weight under HFD feeding, PDE4D KO mice developed comparable insulin resistance compared to controls (Figure S4E, F). More importantly, FGF1 failed to lower blood glucose in these HFD-fed PDE4D KO mice; a defect that was restored with adAAV-driven expression of PDE4D3 in adipose tissue (Figure 4F, G). These data suggest that adipose PDE4D is required for the glucose lowering effects of exogenous FGF1.

### FGF1-induces phosphorylation at a regulatory site on PDE4D3

The activities of phosphodiesterases are regulated by multiple phosphorylation events that integrate different signaling pathways (Mika and Conti, 2016). To explore whether FGF1 signaling induces PDE4D phosphorylation, isoproterenol-stimulated 3T3-L1 adipocytes were treated with FGF1. PDE4D was phosphorylated upon isoproterenol treatment, as evidenced by its decreased mobility in an SDS-PAGE gel (Figure 5A). FGF1 co-treatment increased both the extent and duration of PDE4D phosphorylation (Figure 5A). Consistent with this observation, an increase in PDE4D phosphorylation was seen in gWAT 30 minutes after FGF1 injection (Figure 5B).

PDE4D proteins are phosphorylated by PKA at a conserved S85 site in the upstream conserved region 1 (S54 in humans and rats) that is thought to be necessary for activation, as well as at S44 (S13 in humans and rats), a PDE4D3-specific site in the N-terminus that does not affect PDE activity *in vitro* (Figure 5C) (Hoffmann et al., 1998; Mika and Conti, 2016; Sette and Conti, 1996). To investigate the role of PDE4D3 phosphorylation in the regulation of lipolysis, adAAV expression constructs were generated in which these sites were mutated to alanine. Infection of 3T3-L1 adipocytes with a mutant incorporating S85 to alanine (S85A) largely replicated the ability of wildtype PDE4D3 to suppress lipolysis. In contrast, the S44A mutation abrogated the ability of PDE4D3 to affect lipolysis and HSL phosphorylation (Figure 5D, Figure S5A). Consistent with these findings, a reduced level of isoproterenol-induced phosphorylation was seen with the S44A mutant both in the absence and presence of PDE4 inhibition, implicating a regulatory role for S44 phosphorylation (Figure 5E, Figure S5B). Mutation of both phosphorylation sites (S44A S85A) further

diminished the response to isoproterenol in the presence of a PDE4 inhibitor (treatment with calf intestinal phosphatase (CIP) confirmed that changes in electrophoretic mobility were due to phosphorylation; Figure 5E, Figure S5C). Notably, FGF1-induced phosphorylation of PDE4D3 was lost in the S44A mutant (Figure 5F). Moreover, FGF1 treatment increased S44 phosphorylation in 3T3-L1 cells overexpressing PDE4D3 both in the absence and presence of isoproterenol, as determined using a polyclonal antibody that selectively recognizes PDE4D3 S44 phosphorylation (antibody specificity was confirmed in PDE4D KO gWAT; Figure 5G, Figure S5E, F). WT PDE4D or S44A mutant showed similar *in vitro* PDE catalytic activity when overexpressed in adipocytes, indicating this site does not regulate *in vitro* catalytic activity agreeing with previous findings (Figure S5G) (Carlisle Michel et al., 2004; Dodge et al., 2001). Consistent with a regulatory role of S44 phosphorylation, expression of PDE4D3 but not the S44A mutant restored the ability of FGF1 to suppress lipolysis in PDE4D KO SVF-derived adipocytes (Figure 5H). Mechanistically, FGF1 induced S44 phosphorylation was inhibited by wortmannin in agreement with the dependence of FGF1 anti-lipolytic function on PI3K signaling (Figure 5I, S5H).

The above data indicate that the specific phosphorylation of PDE4D at S44 is required for the anti-lipolytic activity of FGF1/PDE4D pathway. To confirm the *in vivo* relevance of this finding, *ob/ob* mice were injected with adAAV-GFP, adAAV-PDE4D3 or adAAV-PDE4D3 S44A (adipose tissue-specific expression was confirmed by Western blot; Figure S5I). Overexpression of PDE4D3 resulted in lower *ad lib* fed and overnight-fasted blood glucose and serum FFA levels, as well as a trend towards lower insulin levels in the fed state (Figure 5J, 5K, Figure S5J, K). In contrast, overexpression of the S44A mutant failed to affect these metabolic parameters. Importantly, FGF1 induced a greater reduction in glucose levels in mice overexpressing PDE4D3, whereas the response in mice expressing the S44A mutant was indistinguishable from control mice (Figure 5L).

FGF1 was identified as a fed-state adipokine whose expression is increased in response to high fat diet feeding (Jonker et al, 2012). In order to associate endogenous FGF1 signaling with S44 phosphorylation, gWAT depots were collected from chow and HFD fed mice under overnight fasted and re-fed conditions. Re-feeding approximately doubled the pS44 levels in both chow and HFD-fed mice. Interestingly, HFD markedly reduced S44 phosphorylation in both the fasted and fed states, suggestive of a role for PDE4D in insulin-resistant hyperlipidemia (Figure 5M). In combination, these findings support a mechanism in which exogenous FGF1 reduces serum glucose levels by suppressing adipose lipolysis in a PDE4D3-dependent manner, and implicates this mechanism in the physiological response to feeding.

## Discussion

Adipose tissue holds 80–85 % of the body's energy reserves, hence the decision to store or release is central to physiological homeostasis. However, while adipose lipolysis is triggered by multiple factors, insulin is the only known anti-lipolytic regulator. Here we report a signaling cascade induced by FGF1 that functions as an alternate lipolytic suppressive pathway and establishes FGF1 as a regulator of fatty acid homeostasis. Previously, we identified FGF1 as an essential mediator of adipose remodeling (Jonker et al., 2012), and



in subsequent gain-of-function studies, that FGF1 rapidly normalized blood glucose levels in diabetic mouse models in an adipose FGFR1-dependent manner (Suh et al., 2014). In exploring these anti-diabetic activities, we now demonstrate that FGF1-FGFR1 signaling, analogous to insulin signaling, reduces blood glucose levels by suppressing adipose lipolysis and thereby, decreasing HGP through the allosteric regulation of pyruvate carboxylase. Within the adipocyte, FGF1 engages an alternate PI3K/PDE4D circuit to inhibit the cAMP-PKA axis. The resultant reductions in cAMP decrease PKA-mediated phosphorylation of HSL and its subsequent translocation to the lipid droplet. Notably, the PDE4D dependency of the anti-lipolytic and anti-diabetic actions of FGF1 suggest a parallel pathway to the established insulin-PDE3B axis (Figure 6). While both insulin and PKA activate PDE3B via phosphorylation (Degerman et al., 2011), our results reveal a parallel relationship between FGF1 and PDE4D in which phosphorylation of PDE4D3-S44 engages a negative feed-back loop to lower cAMP levels (MacKenzie et al., 2002; Oki et al., 2000; Sette and Conti, 1996). Based on previous studies, convergence of both anti-lipolytic (FGF1) and lipolytic (cAMP/PKA) stimuli on PDE4D phosphorylation suggests a functional compartmentalization of this pathway in different membrane regions as observed with PDE3B regulation (Ahmad et al., 2009).

Mutation of S85 (QRRES motif), which enhances *in vitro* PDE4D3 activity (Sette and Conti, 1996), had a minor effect on suppression of lipolysis when PDE4D3-S85A was overexpressed in adipocytes. This could be explained by excess levels of the PDE4D3-S85A overcoming the inhibitory effects of the point mutation. In contrast, mutation of S44 (FRRHS motif) abrogated the suppression of lipolysis by PDE4D3 despite overexpression, indicating a novel regulatory role for this phosphorylation site. Supporting this notion, over-expression of WT and S44A PDE4D3 resulted in similar PDE activities in adipocytes. Interestingly, the N-terminus of PDE4D3 and its PKA phosphorylation site are implicated in the interaction of PDE4D3 with the muscle-specific A-kinase Anchoring Protein mAKAP (Carlisle Michel *et al.*, 2004; Dodge *et al.*, 2001). Hence, this site may be pivotal in compartmentalization of PKA-PDE4D3 complexes. In addition, binding of phosphatidic acid to the N-terminal sequence has been shown to activate PDE4 (Grange et al., 2000). Future studies are needed to determine the effects of FGF1 on compartmentalized regulation of cAMP signaling and its contribution to lipolysis.

While our work describes the action of FGF1 in adipose tissue, central administration of a single FGF1 dose can also restore glucose homeostasis in diabetic models, however the kinetics are slow (weeks) and the mechanism of action has not been established. The improvement in blood glucose levels in the Zucker T2D diabetic rat model was attributed to preservation of  $\beta$  cell function and increased hepatic glucose uptake, whereas a suppression of the hypothalamic-pituitary-adrenal (HPA) axis resulting in lower lipolysis and hepatic glucose output was described in T1D rats (Perry et al., 2015b; Scarlett et al., 2019; Scarlett et al., 2016). Of note, while the rapid glucose lowering seen with peripheral FGF1 delivery is consistent with lipolytic regulation, the delayed effects of central FGF1 delivery suggest a distinct mechanism.

Our findings implicating adipose PDE4D in the beneficial actions of FGF1 appear at odds with the anti-diabetic effects of systemic PDE4 inhibition (Möllmann et al., 2017;

Vollert et al., 2012). Increased GLP1 secretion, higher serum insulin levels, and increased muscle mitochondrial function have been associated with chronic PDE4 inhibition indicating adipose tissue independent effects. (Ong et al., 2009; Park et al., 2012; Vollert *et al.*, 2012). In addition, contributions of the associated weight loss and potential anti-inflammatory effects of PDE4B inhibition to improvements in glucose tolerance and fasting glucose levels are not known (Jin and Conti, 2002; Komatsu et al., 2013; Möllmann *et al.*, 2017; Zhang *et al.*, 2009). In contrast to the pleiotropic effects of systemic inhibition, our study indicates that PDE4D activity in adipocytes is necessary for FGF1 to suppress lipolysis and lower blood glucose levels (Figure 3 and Figure 4).

PDE3B is important for controlling cAMP levels and lipolysis in adipocytes, however PDE4 accounts for approximately half of the total PDE activity in white adipocytes (Young *et al.*, 2006). Moreover, maximal adipose lipolysis requires both PDE3 and PDE4 inhibitors, supporting an underappreciated role of PDE4 in the regulation of lipolysis (DiPilato et al., 2015b; Kravnik *et al.*, 2013; Snyder *et al.*, 2005). In addition, the finding that FGF1 enhances PDE4D3 phosphorylation at S44 correlates with the post-prandial increases seen at this site in both chow and HFD mice (Figure 5M). The data agree with previous work which showed the anti-lipolytic potential of PDE4 is higher in the fed-state suggesting a potential regulation of PDE4 activity/levels *via* feeding-fasting cycles (Nakamura et al., 2004). Our data indicate the involvement of adipose PDE4D in physiological control of lipolysis *in vivo*. Furthermore, the enhanced lipolysis observed in PDE4D KO mice support this notion. Given that PDE3B levels and activity are decreased in diabetic mouse models, the FGF1/PDE4 regulatory pathway may be increasingly relevant in metabolically stressed states (Tang et al., 2001). This pathway was likely missed because under normal postprandial states, insulin is sufficient to suppress lipolysis and promote fat storage. While logical in retrospect, the idea of a fail-safe anti-lipolytic system had simply not been considered.

Interestingly, the anti-lipolytic effect of FGF1 in the fed state contrasts to FGF21-induced lipolysis in the fasted state. Accordingly, these findings implicate an unexpected FGF1:FGF21 molecular balance regulating the storage and release of fat in the fed and fasted state, respectively. This physiologic paradigm, though seemingly simple, describes a mechanism that not only manages glucose homeostasis in health, but via FGF1 injection, can be used to quickly rebalance glucose levels in insulin resistant type 2 diabetes. Thus, in addition to a new signaling cascade that suppresses lipolysis, these findings reveal the therapeutic potential of the FGF1-PDE4D axis in diabetes.

## Limitations of the study

In exploring the mechanism underlying the acute glucose lowering ability of FGF1, we demonstrate that reduced adipose lipolysis and the associated reduction in free fatty acids results in reduced hepatic glucose production. While the anti-lipolytic activity of FGF1 in adipose tissue is functionally linked to PDE4D, possible contributions from other PDE4 isoforms have not been investigated, and the kinase and/or phosphatase mediating FGF1-induced PDE4D phosphorylation remains to be identified. The extent to which this pathway contributes to the benefits of chronic FGF1 treatment, most notably insulin sensitization, is not fully understood.

## STAR Methods

### Resource availability

**Lead contact**—Further information and requests for resources and reagents should be directed to and will be fulfilled by the Lead Contact, Ronald M. Evans (evans@salk.edu).

**Materials Availability**—Unique reagents generated in this study will be made available upon reasonable request to the Lead Contact with a completed Materials Transfer Agreement.

### Data and Code Availability

- Raw mass-spectrometry data from targeted metabolite measurements has been deposited to MassIVE: MSV000088351.
- No new code has been generated in this study.
- Any additional information required to reanalyze the data reported in this paper is available from the lead contact upon request. All individual data points used in main and supplemental figures are in Table S3.

### Experimental model and subject details

**Mouse model**—Mice were kept in 12h light/dark cycle in a temperature-controlled environment and maintained in accordance with IACUC guidelines complying with US legislation. Mice had free access to food and water unless noted otherwise. C57/B6 mice background was used unless noted otherwise. C57BL/6J and *ob/ob* (000632 - B6. Cg-Lepob/J) male mice were obtained from Jackson Laboratory. PDE4D knock-out mice (034588-UCD) were obtained from MMRRC. For diet-induced obesity (DIO) studies, mice were fed a high fat diet (HFD) (60% fat, F3282; Bio-Serv) for minimum of 12 weeks to induce insulin resistance when diet-induced obese model is used. Insulin levels and blood glucose levels were monitored to confirm insulin resistance. To generate adipose-specific FGFR1 deletion adiponectin-cre mice (B6; FVB-Tg (Adipoq-cre)1Evdrr/J; Stock: 010803) were crossed to *Fgfr1* flox/flox (B6.129S4-Fgfr1tm5.1Sor/J; Stock: 00767) mice. For AAV mediated expression of target proteins in adipose tissue,  $5 \times 10^{11}$  genomic copies of AAV was injected via tail vein or retro-orbital route.

**Cell culture**—All cells were grown at 37°C in a 5% CO<sub>2</sub> humid atmosphere in DMEM, 10% FBS (GemCell,100–500), 1X Antibiotic-Antimycotic (Gibco, 15240096) unless indicated otherwise in method details. 3T3-L1 cells (ATCC, CL-173), mouse SVF-derived cells and human pre-adipocytes (Promocell, C-12735) are differentiated and treated as described in method details section.

### Method details

**Pharmacological studies**—Recombinant FGF1 (rFGF1) was dissolved in phosphate-buffered saline (PBS) at concentration of 0.2 mg/ml was injected subcutaneously at a 0.5 mg kg<sup>-1</sup> dose. Blood glucose was monitored at indicated time points after injection. For initial measurements (2–4 h) food was removed after injection to exclude any indirect effects

stemming from anorexigenic effects of FGF1. PDE4 inhibitor roflumilast stock in DMSO was diluted at 1 mg / ml in 30 % captisol, pH 10 and delivered to mice thorough oral gavage at 5 mg kg<sup>-1</sup> dose. PDE3 inhibitor cilostamide stock in DMSO was diluted at 2 mg / ml in 30 % captisol and delivered through intraperitoneal injection at 10 mg kg<sup>-1</sup> dose.

**Metabolic Studies**—Pyruvate tolerance and glycerol tolerance tests were performed in *ob ob* and DIO mice after overnight fasting at 1.5 g kg<sup>-1</sup> dose using sodium pyruvate (0.2 g/ml) or 20 % glycerol solution in PBS. Insulin tolerance test and glucose tolerance test were performed in *ob ob* mice after 8 h fasting. 2 U kg<sup>-1</sup> insulin (Humulin R) and 0.5 g kg<sup>-1</sup> glucose were used respectively. Blood glucose from tail bleeding was monitored by a OneTouch glucometer.

**Hyperinsulinemic-euglycemic clamps studies.**—Before the test, mice were equipped with a permanent catheter in the right atrium via the jugular vein and were allowed to recover over a period of at least 3 days. After the recovery period, the mice were placed in experimental cages. All infusion experiments were performed in conscious, unrestrained mice as described previously (van Dijk et al., 2003). During the experiment, blood glucose levels were determined every 15 minutes using a Lifescan EuroFlash glucose meter. For GC-MS analysis of [U-13C] glucose, bloodspots on filter paper were collected from the tail vein every 30 minutes.

**Hyperinsulinemic-euglycemic clamp experiment.** *Ob/ob* mice were treated for 1 week with rFGF1 (0.5 mg kg<sup>-1</sup> every other day for one week). Steady state glucose fluxes were determined for basal and hyperinsulinemic-euglycemic clamp conditions. During the first period, mice were infused with a solution containing a tracer of [U-13C] glucose (2.5 mg/ml Cambridge Isotope Laboratories, Andover, MA) at an infusion rate of 0.54 ml/h. With respect to the final period, blood glucose levels were clamped at 20 mM. For this, the mice were infused at a constant rate of 0.135 ml/h with a mixture of insulin (44 mU/ml, Actrapid, Novo Nordisk, Bagsvaerd, Denmark), somatostatin (20 µg/ml, UCB Breda, the Netherlands), 1% BSA, and glucose (200 mg/ml from which 3% [U-13C] glucose). Additionally, a second (variable) infusion was used containing glucose (200 mg/ml from which 3% [U-13C] glucose) to adjust blood glucose levels.

**Targeted metabolomics**—Polar metabolites were extracted and analyzed using a previously reported method (Yuan et al., 2012). Briefly, *ob/ob* mice were sacrificed by cervical dislocation. Liver pieces (50–100 mg) were snap frozen in liquid nitrogen. 1 ml LC-MS grade 80 % methanol chilled at –80°C was added per 100 mg tissue on dry ice. Samples were homogenized by TissueLyzer and lysates were incubated on dry ice for 30 minutes and centrifuged at 20000 g for 10 minutes. Clarified supernatants were transferred to new tubes. Pellets were extracted again and supernatants were combined. After drying the supernatant under nitrogen gas, extracts were dissolved in H<sub>2</sub>O (40 µL) and 10 µL were subjected to liquid chromatography mass spectrometry (LC-MS). Polar metabolites were measured by LC-MS using a TSQ Quantiva instrument fitted with a Luna NH<sub>2</sub> HPLC column (5.0 µm; 4.6 mm x 50 mm, Phenomenex). The following LC solvents were used: buffer A, 95:5 H<sub>2</sub>O/ACN, 20 mM ammonium hydroxide, 20 mM ammonium acetate; buffer

B, 100% ACN. A typical LC run was 23 minutes long with a flow rate of 0.4 ml min<sup>-1</sup> and consisted of the following steps: 85 to 30% buffer B over 3 minutes, 30 to 2% buffer B over 9 minutes, 2% buffer B for 3 minutes, 2 to 85% buffer B over 1 minute, and 85% buffer B for 7 minutes. MS analyses were performed using electrospray ionization (ESI) in negative or positive ion mode depending on the metabolites being analyzed. Negative mode and positive mode source parameters were the following: spray voltage 3.5 kV, ion transfer tube temperature of 325°C, and a vaporizer temperature of 275°C.

**Hepatic pyruvate carboxylase (Pcx) activity assay**—Pcx activity was determined by malate dehydrogenase coupling method originally reported by Payne et al. (Payne and Morris, 1969). Briefly, mice were sacrificed by decapitation. Liver samples were rapidly frozen in liquid nitrogen within 5 seconds of excision designed to avoid loss of hepatic acetyl-CoA levels. Frozen liver samples were pulverized on dry ice and approximately 100 mg of tissues were homogenized with TissueLyzer in Pcx activity assay buffer (50 mM Tris pH8, 10 mM MgCl<sub>2</sub>, 10 mM NaHCO<sub>3</sub>). Homogenates were cleared by centrifugation at 14000 rpm for 10 minutes. Cleared supernatants were diluted in Pcx activity assay buffer to approximately 1 µg/µl. Approximately 5 µg protein was loaded onto 96-well plates and the total volume was brought up to 20 µl by Pcx activity assay buffer. Absorbance at 340 nm was monitored every 9 seconds at 37 °C immediately after the addition of 80 µl Pcx reaction buffer (50 mM Tris pH8, 10 mM MgCl<sub>2</sub>, 10 mM NaHCO<sub>3</sub>, 6.25 mM ATP, 0.125 mM NADH, 2.5 mM pyruvate, malate dehydrogenase 0.025 U/ml in Pcx activity assay buffer). Pcx activity was determined as the loss of absorbance at 340 nm over time normalized to protein concentration.

**Hepatic metabolites quantification**—Liver samples were prepared from HFD-fed mice as described in Pcx activity assay. After determining Pcx activity from sample homogenates, the remaining supernatant was de-proteinated by perchloric acid (PCA)-KOH method using a commercial kit. De-proteinated samples were used to quantify hepatic metabolites using the commercial kits. Hepatic metabolites concentration was normalized to protein concentration and corrected for the loss of volume due to de-proteinization. See “KEY RESOURCES TABLE” for the kits used to determine hepatic metabolites.

**Adipose transplantation**—8-week old F1WT mice were sacrificed. Their gonadal adipose tissue (gWAT) was excised into small pieces (approximately 3 mm x 3 mm) and maintained in saline briefly. Age-matched 8-week old F1WT and F1KO mice were anesthetized by ketamine/xylazine solution (80 mg kg<sup>-1</sup> and 10 mg kg<sup>-1</sup>, respectively). Multiple small incisions in dorsum were made in anesthetized mice and a piece of gWAT from F1WT was placed inside each incision. Each recipient mouse received the entire gWAT from the donor mouse. Wounds were closed by wound clip. Mice were allowed to recover on heat pad. Mice were monitored, and antibiotics and pain medicine (Ibuprofen) were provided post-surgery for 3 days. 2 weeks after surgery, recipient mice were sacrificed either under 6-hour refeed condition.

**Isolation of adipose stromal vascular fraction**—Isolation of adipose stromal fraction (SVF) was performed as published previously with slight modifications (Bapat et al.,

2015). Inguinal adipose (iWAT) tissues were used for isolation of SVF due their ability to differentiate to mature adipocytes. Briefly, adipose tissues were dissected, washed in cold PBS and cut into small pieces in digestion buffer (100 mM HEPES, 120 mM NaCl, 50 mM KCl, 1 mM CaCl<sub>2</sub>, 1.5% fatty acids free BSA, 1 mg/ml collagenase I). Samples were dissociated in 37 °C water bath with shaking for 30–60 min with occasional monitoring to prevent over digestion. Tissue debris were filtered by 100 µm cell strainer and SVF was collected by centrifugation at 500 g for 5 minutes. Cell pellet was washed once by PBS and filtered with 40 µm cell strainer. Red blood cells were lysed with Red blood cell lysis buffer (BioLegend) according to manufacturer's instructions. The remaining cells were re-suspended and cultured in DMEM/F12 with 20 % FBS (GemCell,100–500) at 37 °C, 5 % CO<sub>2</sub>.

***In vitro* differentiation of adipocytes**—Differentiation of pre-adipocytes were based on previously published methods (Bunnell et al., 2008). Briefly, 3T3-L1 pre-adipocytes were grown to full confluence in DMEM, 10 % FBS (GemCell,100–500), 10 mM HEPES and antibiotic-antimycotic (full growth media). 2 days later, differentiation was induced by replacing the media with 1 µM dexamethasone, 1 µM rosiglitazone, 500 µM IBMX and 5 µg / ml insulin in full growth media 2 days later after reaching full confluence. 2 days later media is replaced by differentiation induction media with 1 µM rosiglitazone and 5 µg / ml insulin for 4 days with media change after 2 days. Cells were kept in maintenance medium (full growth media with 5 µg / ml insulin) for 4 more days for full differentiation. For differentiation of mouse SVF derived adipocytes, protocol was same except DMEM/F12 (10565018, ThermoFisher) was used as base media and initial differentiation induction media was kept 3 days. For differentiation of human subcutaneous adipocytes, protocol and media from the manufacturer (C-12735, C-39437, Promocell) were used. Dexamethasone was omitted from the media in the last 3 days before performing experiments. Both mouse and human SVF derived adipocytes were differentiated in collagen coated plates (A1142802, ThermoFisher).

**Lipolysis assays**—For *in vitro* lipolysis assay, cells were washed with PBS and media were changed to full growth media 1 day before experiment. Cells were serum starved for 2 h and placed in KRBH buffer (30 mM HEPES, 120 mM NaCl, 4 mM KH<sub>2</sub>PO<sub>4</sub>, 1 mM MgSO<sub>4</sub>, 0.75 mM CaCl<sub>2</sub>, and 10 mM NaHCO<sub>3</sub>) with 2 % fatty acid free BSA and 5 mM glucose. FGF1 was added 10 min before induction of lipolysis with 100 nM isoproterenol (ISO). Inhibitors were added 30 min prior to FGF1 treatment unless otherwise noted. Media were collected and cells were lysed in protein extraction buffer. FFAs were measured in the media using commercial kit (Wako-NEFAHR2) and normalized to protein concentration. For *ex vivo* lipolysis, the assay was modified from a published protocol (Funicello et al., 2007). Briefly, approximately 0.1 gram of adipose tissue were excised, weighted and kept in cold PBS until treatment and control tissues were collected. Tissues were cut into small pieces and incubated in same KRBH buffer as described above for 4 h. FFAs were measured and normalized by the explant weights.

**Protein extraction and Immunoblotting**—Tissues were lysed in cold lysis buffer (50 mM Tris, pH 7.5, 150 mM NaCl, 1 % NP40, 0.5 % NaDoc, 0.1 % SDS, 5 % glycerol,

1 mM EDTA, protease and phosphatase inhibitors (cOmplete and PhosSTOP (Roche)) by homogenization by bead-beater for 30 s. Samples were cleared for 10 min at 18000 g at 4 °C middle clear phase is transferred to new tubes. A second 30 min centrifugation was performed and middle clear phase is transferred to new tubes. 5 µl protein extract was used for BCA assay to determine protein concentration. Samples were boiled in laemmli buffer. SDS-PAGE and blotting were performed using gradient gels and Trans-Blot Turbo Transfer System (Bio-Rad). Antibodies used were PDE4D (12918–1-AP, Proteintech), pHSL-660 (4126S, Cell signaling), HSL (4107S, Cell Signaling), tubulin (CP06, Millipore Sigma), GFP (A01388, GenScript). PDE4D3-pS44 phospho-specific antibody was generated using PDE4D3-S44 FRRHpSWISFDVDNGTSAGR peptide (MacKenzie *et al.*, 2002) by Pocono Rabbit Farm, using 70-day rabbit antibody production protocol and purified via affinity purification. Primary antibodies were incubated 2h RT or ON at 4 °C. Blots were developed using SuperSignal West Pico PLUS Chemiluminescent Substrate (ThermoFisher Scientific) and imaged with BioRad GelDoc system.

#### **Molecular cloning and production of adenoviral/adeno-associated virus—**

Virapower gateway adenovirus expression kit was used to clone ORFs of various isoforms of mouse PDE4D (XM\_006517645.4, XM\_030247262.1 and XM\_006517647.3) to adenoviral vectors according to manufacturer's protocol. Vectors were transfected to 293A cell line using Fugene transfection reagent (PRE2692, Promega). Crude adenovirus stock was used to infect new 293A cells for large-scale adenovirus production. Transduced 293A cells were harvested when cytopathic effect was apparent 2–3 days after inoculation with crude adenovirus stock. Virus were purified via adenovirus standard purification kit (3054, Virapur). For adipose specific expression of target proteins by AAV mediated transduction (adAAV), vector was designed by using human adiponectin promoter/enhancer based on O'neil et al (O'Neill *et al.*, 2014) and 4X repeat miRNA target for mir122T (Qiao *et al.*, 2011) after cloned ORF to further prevent liver expression. adAAV backbone was synthesized by Vector Builder. ORFs of PDE4D3, GFP, mCherry, Perilipin-GFP, HSL-mCherry were cloned to the vector with standard restriction digestion cloning. cDNA from gonadal adipose tissue was used to amplify the ORFs with the primers listed at Table S2. Stabl3 cells were used for vector amplification and Hi Pure Purelink Expi Plasmid Giga Prep (ThermoFisher) was used for AAV vector purification. Large scale AAV8 production and calculation of the titer were performed by Salk Institute Gene Transfer, Targeting, and Therapeutics Core (GT3). Mutagenesis experiments were performed by using QuickChange XL Site-Directed Mutagenesis Kit (200517, Agilent). Primer sequences are listed at Table S2.

**PDE Assay—**PDE activities were measured by using [3H]-labelled cAMP as described previously with slight modifications (Rybalkin *et al.*, 2013). Briefly, 10 µg of protein extract is incubated in assay buffer (20 mM Tris pH 7.4, 0.8mM EGTA pH 8, 0.2 mg/ml BSA, 15 mM magnesium acetate, 1 µM cAMP, 50000 cpm [3H]-cAMP) in 250 µl volume at 30°C for 15 min. Reaction is stopped by adding 125µl, 0.25M HCl and neutralized by adding 125ul 0.25M NaOH and final 100 mM Tris-HCl pH 7.4. 5µl Crotalus atrox venom (BML-KI307) is used for dephosphorylation of [3 H]-5- AMP at 30°C for 30 min. [3 H]-adenosine product was separated from [3H]-cAMP substrate by ion-exchange

chromatography (DEAE-Sephadex A-25; GE Healthcare) and quantified by scintillation counting.

**Microscopy**—3T3-L1 cells were transduced with viral particles ( $10^4$  –  $10^6$  GC /cell) in 24 well plates. Media were replaced after overnight incubation. 3–4 days after AAV infection, cells were treated as described in lipolysis assay. For cAMP analysis by biosensors, Downward Green cADDis cAMP Sensor (D0200G) and control mNeon Green (F0500G) produced in BacMam system was purchased from Montana molecular. Brightfield and fluorescence images were taken every 10–20 min in IncuCyte Live-cell analysis system (Sartorius) and images were analyzed by IncuCyte® Analysis Software. High-resolution live cell imaging was performed with LSM 880 Airyscan microscope at 40X objective.

**Replication and randomization:** Animal experiments were performed on multiple cohorts. In vitro experiments were performed at least 3 times. The randomized block design was used for all animal experiments. We identified the age, sex, body weight and cage effect as blocking factors. Therefore, all animal experiments were carried out on age-matched animals of the same sex. Body weight were measured before assigning treatment groups. Cage effect was controlled in pharmacological treatment studies by assigning animals to the placebo or treatment group from the same cage.

**Quantification and statistical analysis**—Pre-determined sample exclusion criterion is established for technical failures. Unless otherwise noted, statistical significance was calculated by unpaired, two-tailed student's t test. In time series data, two-way ANOVA was performed. Data are presented as mean  $\pm$  SEM.

## Supplementary Material

Refer to Web version on PubMed Central for supplementary material.

## Acknowledgements

We thank Z. Wei, N. He, W. Fan, B. Lu, T. Fu, K. Kim, T. G. Oh, H. Song, B. Henriquez, D. Wang, L. Chong, G. Estapa, M. He, D. Struik, and H. Juguilon for technical assistance, and L. Ong and C. Brondos for administrative assistance. This work was supported by grants from NIH (DK057978) and the Nomis Foundation. R.M.E. is a March of Dimes Chair in Molecular and Developmental Biology at the Salk Institute. G.S. was supported by a Deutsche Forschungsgemeinschaft (DFG) postdoctoral fellowship (SA 2991/1–1) and J.W.J. was supported by grants from The Netherlands Organization for Scientific Research (VICI grant 016.176.640 to J.W.J) and the European Foundation for the Study of Diabetes (award supported by EFSD/Novo Nordisk to J.W.J). E.G. was supported by a Swiss National Science Foundation (SNF) fellowship (P400PM\_180759). This work was supported by the Mass Spectrometry Core of the Salk Institute with funding from NIH-NCI CCSG: P30 014195 and the Helmsley Center for Genomic Medicine. Research reported in the publication was supported by the National Heart, Lung and Blood Institute (NHLBI) of the National Institute of Health under Award Number P01HL147835, by the National Institute of Diabetes and Digestive and Kidney Diseases (NIDDK) of the National Institutes of Health under Award Number R01DK057978, and by the National Institute of Environmental Health Sciences (NIEHS) of the National Institutes of Health under Award Number P42ES010337. The content is solely the responsibility of the authors and does not necessarily represent the official views of the National Institutes of Health. Figure 6 and graphical abstract were created with [BioRender.com](https://BioRender.com).

## References

Ahmad F, Lindh R, Tang Y, Ruishalme I, Ost A, Sahachartsiri B, Strålfors P, Degerman E, and Manganiello VC (2009). Differential regulation of adipocyte PDE3B in distinct membrane



compartments by insulin and the beta3-adrenergic receptor agonist CL316243: effects of caveolin-1 knockdown on formation/maintenance of macromolecular signalling complexes. *Biochem J* 424, 399–410. 10.1042/BJ20090842. [PubMed: 19747167]

Azevedo MF, Faucz FR, Bimpaki E, Horvath A, Levy I, de Alexandre RB, Ahmad F, Manganiello V, and Stratakis CA (2014). Clinical and molecular genetics of the phosphodiesterases (PDEs). *Endocr Rev* 35, 195–233. 10.1210/er.2013-1053. [PubMed: 24311737]

Baeza-Raja B, Sachs BD, Li P, Christian F, Vagena E, Davalos D, Le Moan N, Ryu JK, Sikorski SL, Chan JP, et al. (2016). p75 Neurotrophin Receptor Regulates Energy Balance in Obesity. *Cell Rep* 14, 255–268. 10.1016/j.celrep.2015.12.028. [PubMed: 26748707]

Bapat SP, Myoung Suh J, Fang S, Liu S, Zhang Y, Cheng A, Zhou C, Liang Y, LeBlanc M, Liddle C, et al. (2015). Depletion of fat-resident Treg cells prevents age-associated insulin resistance. *Nature* 528, 137–141. 10.1038/nature16151. [PubMed: 26580014]

Bartness TJ, Liu Y, Shrestha YB, and Ryu V (2014). Neural innervation of white adipose tissue and the control of lipolysis. *Front Neuroendocrinol* 35, 473–493. 10.1016/j.yfrne.2014.04.001. [PubMed: 24736043]

Boden G, Chen X, and Stein TP (2017). Gluconeogenesis in moderately and severely hyperglycemic patients with type 2 diabetes mellitus. *American Journal of Physiology-Endocrinology and Metabolism*. 10.1152/ajpendo.2001.280.1.e23.

Bunnell BA, Flaata M, Gagliardi C, Patel B, and Ripoll C (2008). Adipose-derived stem cells: isolation, expansion and differentiation. *Methods* 45, 115–120. 10.1016/j.ymeth.2008.03.006. [PubMed: 18593609]

Carlisle Michel JJ, Dodge KL, Wong W, Mayer NC, Langeberg LK, and Scott JD (2004). PKA-phosphorylation of PDE4D3 facilitates recruitment of the mAKAP signalling complex. *Biochemical Journal*. 10.1042/BJ20040846.

Choi Y, Jang S, Choi MS, Ryoo ZY, and Park T (2016). Increased expression of FGF1-mediated signaling molecules in adipose tissue of obese mice. *J Physiol Biochem* 72, 157–167. 10.1007/s13105-016-0468-6. [PubMed: 26847131]

Clifford GM, Londos C, Kraemer FB, Vernon RG, and Yeaman SJ (2000). Translocation of hormone-sensitive lipase and perilipin upon lipolytic stimulation of rat adipocytes. *Journal of Biological Chemistry*. 10.1074/jbc.275.7.5011.

Degerman E, Ahmad F, Chung YW, Guirguis E, Omar B, Stenson L, and Manganiello V (2011). From PDE3B to the regulation of energy homeostasis. *Curr Opin Pharmacol* 11, 676–682. 10.1016/j.coph.2011.09.015. [PubMed: 22001403]

DiPilato LM, Ahmad F, Harms M, Seale P, Manganiello V, and Birnbaum MJ (2015a). The Role of PDE3B Phosphorylation in the Inhibition of Lipolysis by Insulin. *Mol Cell Biol* 35, 2752–2760. 10.1128/MCB.00422-15. [PubMed: 26031333]

DiPilato LM, Ahmad F, Harms M, Seale P, Manganiello V, and Birnbaum MJ (2015b). The Role of PDE3B Phosphorylation in the Inhibition of Lipolysis by Insulin. *Molecular and Cellular Biology*. 10.1128/mcb.00422-15.

Dipilato LM, Ahmad F, Harms M, Seale P, Manganiello V, and Birnbaum MJ (2015). The Role of PDE3B Phosphorylation in the Inhibition of Lipolysis by Insulin. 35. 10.1128/MCB.00422-15.

Dodge KL, Khouangathiene S, Kapiloff MS, Mouton R, Hill EV, Houslay MD, Langeberg LK, and Scott JD (2001). mAKAP assembles a protein kinase A/PDE4 phosphodiesterase cAMP signaling module. *EMBO Journal*. 10.1093/emboj/20.8.1921.

Duncan RE, Ahmadian M, Jaworski K, Sarkadi-Nagy E, and Sul HS (2007). Regulation of lipolysis in adipocytes. *Annu Rev Nutr* 27, 79–101. 10.1146/annurev.nutr.27.061406.093734. [PubMed: 17313320]

Egan JJ, Greenberg AS, Chang MK, Wek SA, Moos MC, and Londos C (1992). Mechanism of hormone-stimulated lipolysis in adipocytes: translocation of hormone-sensitive lipase to the lipid storage droplet. *Proceedings of the National Academy of Sciences*. 10.1073/pnas.89.18.8537.

Exton JH, and Park CR (1967). Control of gluconeogenesis in liver. I. General features of gluconeogenesis in the perfused livers of rats. *Journal of Biological Chemistry*.

Funicello M, Novelli M, Ragni M, Vottari T, Cocuzza C, Soriano-Lopez J, Chiellini C, Boschi F, Marzola P, Masiello P, et al. (2007). Cathepsin K null mice show reduced adiposity during the

- rapid accumulation of fat stores. *PLoS One* 2, e683. 10.1371/journal.pone.0000683. [PubMed: 17668061]
- Grange M, Sette C, Cuomo M, Conti M, Lagarde M, Prigent A-F, and Némoz G (2000). The cAMP-specific Phosphodiesterase PDE4D3 Is Regulated by Phosphatidic Acid Binding. *Journal of Biological Chemistry*. 10.1074/jbc.m006329200.
- Greenberg AS, Egan JJ, Wek SA, Garty NB, Blanchette-Mackie EJ, and Londos C (1991). Perilipin, a major hormonally regulated adipocyte-specific phosphoprotein associated with the periphery of lipid storage droplets. *Journal of Biological Chemistry*.
- Grønning LM, Baillie GS, Cederberg A, Lynch MJ, Houslay MD, Enerbäck S, and Taskén K (2006). Reduced PDE4 expression and activity contributes to enhanced catecholamine-induced cAMP accumulation in adipocytes from FOXC2 transgenic mice. *FEBS Lett* 580, 4126–4130. 10.1016/j.febslet.2006.06.058. [PubMed: 16828089]
- Hoffmann R, Wilkinson IR, McCallum JF, Engels P, and Houslay MD (1998). cAMP-specific phosphodiesterase HSPDE4D3 mutants which mimic activation and changes in rolipram inhibition triggered by protein kinase A phosphorylation of Ser-54: generation of a molecular model. *Biochem J* 333 ( Pt 1), 139–149. 10.1042/bj3330139. [PubMed: 9639573]
- Houslay MD, and Adams DR (2003). PDE4 cAMP phosphodiesterases: modular enzymes that orchestrate signalling cross-talk, desensitization and compartmentalization. *Biochem J* 370, 1–18. 10.1042/BJ20021698. [PubMed: 12444918]
- Inagaki T, Dutchak P, Zhao G, Ding X, Gautron L, Parameswara V, Li Y, Goetz R, Mohammadi M, Esser V, et al. (2007). Endocrine regulation of the fasting response by PPAR $\alpha$ -mediated induction of fibroblast growth factor 21. *Cell Metab* 5, 415–425. 10.1016/j.cmet.2007.05.003. [PubMed: 17550777]
- Jang MH, Mukherjee S, Choi MJ, Kang NH, Pham HG, and Yun JW (2020). Theobromine alleviates diet-induced obesity in mice via phosphodiesterase-4 inhibition. *Eur J Nutr* 59, 3503–3516. 10.1007/s00394-020-02184-6. [PubMed: 31965293]
- Jin SL, and Conti M (2002). Induction of the cyclic nucleotide phosphodiesterase PDE4B is essential for LPS-activated TNF- $\alpha$  responses. *Proc Natl Acad Sci U S A* 99, 7628–7633. 10.1073/pnas.122041599. [PubMed: 12032334]
- Jin SL, Lan L, Zoudilova M, and Conti M (2005). Specific role of phosphodiesterase 4B in lipopolysaccharide-induced signaling in mouse macrophages. *J Immunol* 175, 1523–1531. 10.4049/jimmunol.175.3.1523. [PubMed: 16034090]
- Jin SL, Richard FJ, Kuo WP, D'Ercole AJ, and Conti M (1999). Impaired growth and fertility of cAMP-specific phosphodiesterase PDE4D-deficient mice. *Proc Natl Acad Sci U S A* 96, 11998–12003. 10.1073/pnas.96.21.11998. [PubMed: 10518565]
- Jonker JW, Suh JM, Atkins AR, Ahmadian M, Li P, Whyte J, He M, Juguilon H, Yin YQ, Phillips CT, et al. (2012). A PPAR $\gamma$ -FGF1 axis is required for adaptive adipose remodelling and metabolic homeostasis. *Nature* 485, 391–394. 10.1038/nature10998. [PubMed: 22522926]
- Kitamura T, Kitamura Y, Kuroda S, Hino Y, Ando M, Kotani K, Konishi H, Matsuzaki H, Kikkawa U, Ogawa W, and Kasuga M (1999). Insulin-induced phosphorylation and activation of cyclic nucleotide phosphodiesterase 3B by the serine-threonine kinase Akt. *Mol Cell Biol* 19, 6286–6296. 10.1128/mcb.19.9.6286. [PubMed: 10454575]
- Komatsu K, Lee JY, Miyata M, Hyang Lim J, Jono H, Koga T, Xu H, Yan C, Kai H, and Li JD (2013). Inhibition of PDE4B suppresses inflammation by increasing expression of the deubiquitinase CYLD. *Nat Commun* 4, 1684. 10.1038/ncomms2674. [PubMed: 23575688]
- Kraynik SM, Miyaoka RS, and Beavo JA (2013). PDE3 and PDE4 Isozyme-Selective Inhibitors Are Both Required for Synergistic Activation of Brown Adipose Tissue s. 4, 1155–1165.
- Lin HV, and Accili D (2011). Hormonal regulation of hepatic glucose production in health and disease.
- Lombardo YB, and Menahan LA (1979). Gluconeogenesis in perfused livers of genetically obese-hyperglycemic (ob/ob) mice. *Hormone and Metabolic Research*. 10.1055/s-0028-1092672.
- MacKenzie SJ, Baillie GS, McPhee I, MacKenzie C, Seamons R, McSorley T, Millen J, Beard MB, van Heeke G, and Houslay MD (2002). Long PDE4 cAMP specific phosphodiesterases are activated by protein kinase A-mediated phosphorylation of a single serine residue in Upstream

- Conserved Region 1 (UCR1). *Br J Pharmacol* 136, 421–433. 10.1038/sj.bjp.0704743. [PubMed: 12023945]
- Mika D, and Conti M (2016). PDE4D phosphorylation: A coincidence detector integrating multiple signaling pathways.
- Möllmann J, Kahles F, Lebherz C, Kappel B, Baeck C, Tacke F, Werner C, Federici M, Marx N, and Lehrke M (2017). The PDE4 inhibitor roflumilast reduces weight gain by increasing energy expenditure and leads to improved glucose metabolism. *Diabetes Obes Metab* 19, 496–508. 10.1111/dom.12839. [PubMed: 27917591]
- Nakamura J, Okamura N, and Kawakami Y (2004). Augmentation of lipolysis in adipocytes from fed rats, but not from starved rats, by inhibition of rolipram-sensitive phosphodiesterase 4. 425, 106–114. 10.1016/j.abb.2004.02.036.
- O'Neill SM, Hinkle C, Chen SJ, Sandhu A, Hovhannisyan R, Stephan S, Lagor WR, Ahima RS, Johnston JC, and Reilly MP (2014). Targeting adipose tissue via systemic gene therapy. *Gene Therapy*. 10.1038/gt.2014.38.
- Oki N, Takahashi SI, Hidaka H, and Conti M (2000). Short term feedback regulation of cAMP in FRTL-5 thyroid cells. Role of PDE4D3 phosphodiesterase activation. *J Biol Chem* 275, 10831–10837. 10.1074/jbc.275.15.10831. [PubMed: 10753877]
- Oknianska A, Zmuda-Trzebiatowska E, Manganiello V, and Degerman E (2007). Long-term regulation of cyclic nucleotide phosphodiesterase type 3B and 4 in 3T3-L1 adipocytes. *Biochem Biophys Res Commun* 353, 1080–1085. 10.1016/j.bbrc.2006.12.141. [PubMed: 17198676]
- Ong WK, Gribble FM, Reimann F, Lynch MJ, Houslay MD, Baillie GS, Furman BL, and Pyne NJ (2009). The role of the PDE4D cAMP phosphodiesterase in the regulation of glucagon-like peptide-1 release. *British Journal of Pharmacology*. 10.1111/j.1476-5381.2009.00194.x.
- Park SJ, Ahmad F, Philp A, Baar K, Williams T, Luo H, Ke H, Rehmann H, Taussig R, Brown AL, et al. (2012). Resveratrol ameliorates aging-related metabolic phenotypes by inhibiting cAMP phosphodiesterases. *Cell*. 10.1016/j.cell.2012.01.017.
- Payne J, and Morris JG (1969). Pyruvate carboxylase in *Rhodospseudomonas spheroides*. *J Gen Microbiol* 59, 97–101. 10.1099/00221287-59-1-97. [PubMed: 5365367]
- Perry RJ, Camporez JG, Kursawe R, Titchenell PM, Zhang D, Perry CJ, Jurczak MJ, Abudukadier A, Han MS, Zhang XM, et al. (2015a). Hepatic acetyl CoA links adipose tissue inflammation to hepatic insulin resistance and type 2 diabetes. *Cell* 160, 745–758. 10.1016/j.cell.2015.01.012. [PubMed: 25662011]
- Perry RJ, Lee S, Ma L, Zhang D, Schlessinger J, and Shulman GI (2015b). FGF1 and FGF19 reverse diabetes by suppression of the hypothalamic-pituitary-adrenal axis. *Nat Commun* 6, 6980. 10.1038/ncomms7980. [PubMed: 25916467]
- Perry RJ, Wang Y, Cline GW, Rabin-Court A, Song JD, Dufour S, Zhang XM, Petersen KF, and Shulman GI (2018). Leptin Mediates a Glucose-Fatty Acid Cycle to Maintain Glucose Homeostasis in Starvation. *Cell* 172, 234–248.e217. 10.1016/j.cell.2017.12.001. [PubMed: 29307489]
- Qiao C, Yuan Z, Li J, He B, Zheng H, Mayer C, and Xiao X (2011). Liver-specific microRNA-122 target sequences incorporated in AAV vectors efficiently inhibits transgene expression in the liver. *Gene Therapy*. 10.1038/gt.2010.157.
- Rahn T, Ridderstråle M, Tornqvist H, Manganiello V, Fredrikson G, Belfrage P, and Degerman E (1994). Essential role of phosphatidylinositol 3-kinase in insulin-induced activation and phosphorylation of the cGMP-inhibited cAMP phosphodiesterase in rat adipocytes. Studies using the selective inhibitor wortmannin. *FEBS Lett* 350, 314–318. 10.1016/0014-5793(94)00797-7. [PubMed: 8070584]
- Rebrin K, Steil GM, Mittelman SD, and Bergman RN (1996). Causal linkage between insulin suppression of lipolysis and suppression of liver glucose output in dogs. *J Clin Invest* 98, 741–749. 10.1172/JCI118846. [PubMed: 8698866]
- Rybalkin SD, Hinds TR, and Beavo JA (2013). Enzyme assays for cGMP hydrolyzing phosphodiesterases. *Methods Mol Biol* 1020, 51–62. 10.1007/978-1-62703-459-3\_3. [PubMed: 23709025]

- Saponaro C, Gaggini M, Carli F, and Gastaldelli A (2015). The Subtle Balance between Lipolysis and Lipogenesis: A Critical Point in Metabolic Homeostasis. *Nutrients* 7, 9453–9474. 10.3390/nu7115475. [PubMed: 26580649]
- Scarlett JM, Muta K, Brown JM, Rojas JM, Matsen ME, Acharya NK, Secher A, Ingvorsen C, Jorgensen R, Høeg-Jensen T, et al. (2019). Peripheral Mechanisms Mediating the Sustained Antidiabetic Action of FGF1 in the Brain. *Diabetes* 68, 654–664. 10.2337/db18-0498. [PubMed: 30523024]
- Scarlett JM, Rojas JM, Matsen ME, Kaiyala KJ, Stefanovski D, Bergman RN, Nguyen HT, Dorfman MD, Lantier L, Wasserman DH, et al. (2016). Central injection of fibroblast growth factor 1 induces sustained remission of diabetic hyperglycemia in rodents. *Nat Med* 22, 800–806. 10.1038/nm.4101. [PubMed: 27213816]
- Sears B, and Perry M (2015). The role of fatty acids in insulin resistance. *Lipids Health Dis* 14, 121. 10.1186/s12944-015-0123-1. [PubMed: 26415887]
- Sette C, and Conti M (1996). Phosphorylation and activation of a cAMP-specific phosphodiesterase by the cAMP-dependent protein kinase. Involvement of serine 54 in the enzyme activation. *J Biol Chem* 271, 16526–16534. 10.1074/jbc.271.28.16526. [PubMed: 8663227]
- Shen W-J, Patel S, Miyoshi H, Greenberg AS, and Kraemer FB (2009). Functional interaction of hormone-sensitive lipase and perilipin in lipolysis. *Journal of Lipid Research*. 10.1194/jlr.M900176-jlr200.
- Shrago E, and Lardy HA (1966). Paths of carbon in gluconeogenesis and lipogenesis. II. Conversion of precursors to phosphoenolpyruvate in liver cytosol. *Journal of Biological Chemistry*.
- Snyder PB, Esselstyn JM, Loughney K, Wolda SL, Florio VA, and Corporation I (2005). The role of cyclic nucleotide phosphodiesterases in the regulation of adipocyte lipolysis. 46. 10.1194/jlr.M400362-JLR200.
- Strålfors P, and Honnor RC (1989). Insulin-induced dephosphorylation of hormone-sensitive lipase. Correlation with lipolysis and cAMP-dependent protein kinase activity. *Eur J Biochem* 182, 379–385. 10.1111/j.1432-1033.1989.tb14842.x. [PubMed: 2661229]
- Suh JM, Jonker JW, Ahmadian M, Goetz R, Lackey D, Osborn O, Huang Z, Liu W, Yoshihara E, Van Dijk TH, et al. (2014). Endocrinization of FGF1 produces a neomorphic and potent insulin sensitizer. *Nature* 513, 436–439. 10.1038/nature13540. [PubMed: 25043058]
- Tang Y, Osawa H, Onuma H, Nishimiya T, Ochi M, Sugita A, and Makino H (2001). Phosphodiesterase 3B gene expression is enhanced in the liver but reduced in the adipose tissue of obese insulin resistant db/db mouse. *Diabetes Res Clin Pract* 54, 145–155. 10.1016/s0168-8227(01)00271-6. [PubMed: 11689269]
- Tewson PH, Martinka S, Shaner NC, Hughes TE, and Quinn AM (2016). New DAG and cAMP Sensors Optimized for Live-Cell Assays in Automated Laboratories. *J Biomol Screen* 21, 298–305. 10.1177/1087057115618608. [PubMed: 26657040]
- Turner SM, Linfoot PA, Neese RA, and Hellerstein MK (2005). Sources of plasma glucose and liver glycogen in fasted ob/ob mice. *Acta Diabetologica*. 10.1007/s00592-005-0201-3.
- van Dijk TH, Boer TS, Havinga R, Stellaard F, Kuipers F, and Reijngoud DJ (2003). Quantification of hepatic carbohydrate metabolism in conscious mice using serial blood and urine spots. *Anal Biochem* 322, 1–13. 10.1016/j.ab.2003.07.008. [PubMed: 14705774]
- Vollert S, Kaessner N, Heuser A, Hanauer G, Dieckmann A, Knaack D, Kley HP, Beume R, and Weiss-Haljiti C (2012). The glucose-lowering effects of the PDE4 inhibitors roflumilast and roflumilast-N-oxide in db/db mice. *Diabetologia*. 10.1007/s00125-012-2632-z.
- Wang S, Cao S, Arhatte M, Li D, Shi Y, Kurz S, Hu J, Wang L, Shao J, Atzberger A, et al. (2020). Adipocyte Piezo1 mediates obesogenic adipogenesis through the FGF1/FGFR1 signaling pathway in mice. *Nat Commun* 11, 2303. 10.1038/s41467-020-16026-w. [PubMed: 32385276]
- Young HC, Park S, Hockman S, Zmuda-Trzebiatowska E, Svannelid F, Haluzik M, Gavrilova O, Ahmad F, Pepin L, Napolitano M, et al. (2006). Alterations in regulation of energy homeostasis in cyclic nucleotide phosphodiesterase 3B-null mice. *Journal of Clinical Investigation*. 10.1172/JCI24867.

- Yuan M, Breitkopf SB, Yang X, and Asara JM (2012). A positive/negative ion-switching, targeted mass spectrometry-based metabolomics platform for bodily fluids, cells, and fresh and fixed tissue. *Nat Protoc* 7, 872–881. 10.1038/nprot.2012.024. [PubMed: 22498707]
- Zhang R, Maratos-Flier E, and Flier JS (2009). Reduced adiposity and high-fat diet-induced adipose inflammation in mice deficient for phosphodiesterase 4B. *Endocrinology* 150, 3076–3082. 10.1210/en.2009-0108. [PubMed: 19359377]

Author Manuscript

Author Manuscript

Author Manuscript

Author Manuscript

### Highlights

- FGF1-FGFR1 signaling suppresses adipose lipolysis to curb hepatic glucose production
- FGF1 suppresses lipolysis by inhibiting cAMP/PKA axis *via* PDE4D-S44 phosphorylation
- Over-expression of PDE4D in the adipose tissue of diabetic mice corrects hyperglycemia
- FGF1/PDE4D antilipolytic pathway is responsive to fed/fast states

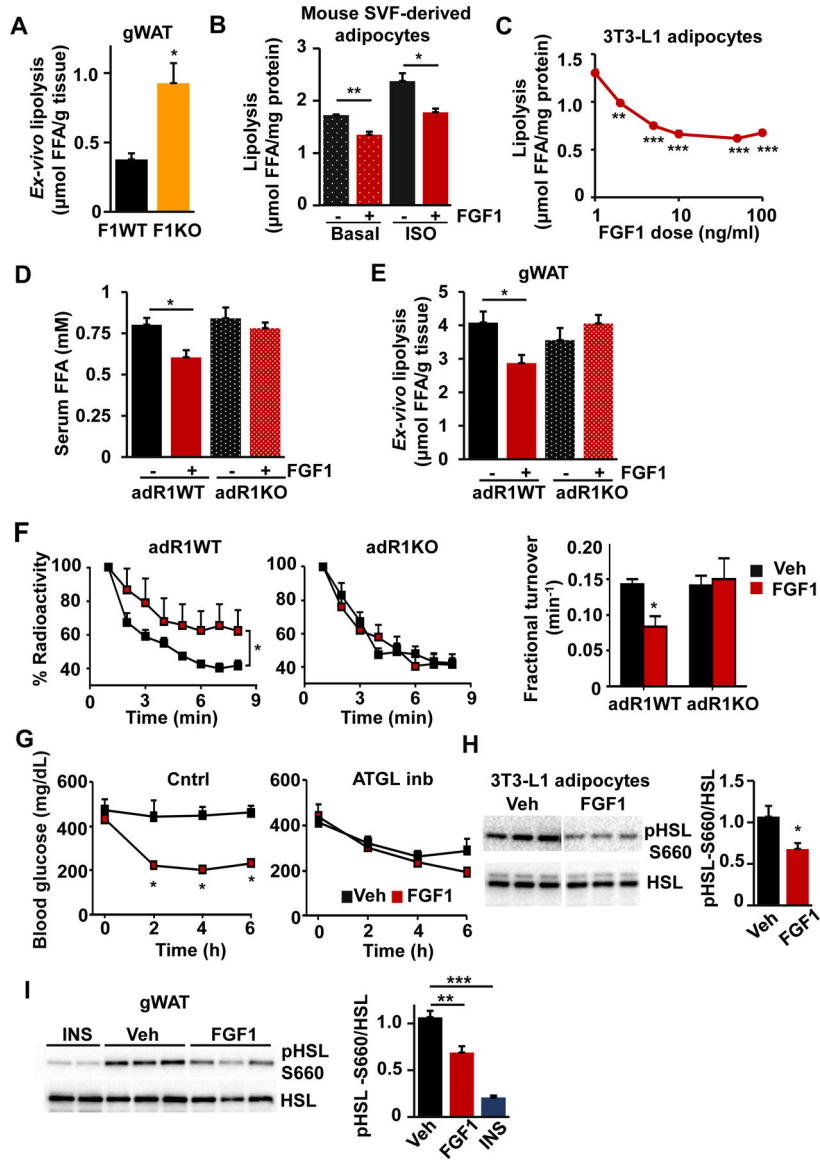


**Figure 1. FGF1 suppresses adipose lipolysis**

A) *Ex-vivo* lipolysis in gonadal white adipose tissue (gWAT) explants from wildtype (F1WT) and FGF1 KO (F1KO) mice 6 h after refeeding. Data are represented as mean  $\pm$  SEM (n=4, \* $p$  < 0.05).

B) Lipolysis in mouse SVF-derived adipocytes measured by the cumulative release of free fatty acids (FFAs) into the media over 4 h. Cells were pretreated with vehicle (PBS) or FGF1 (100 ng/ml) for 10 min prior to the induction of lipolysis with 1 nM isoproterenol (ISO). Data are represented as mean  $\pm$  SEM (n = 3, \* $p$  < 0.05, \*\* $p$  < 0.01).

C) Dose response of FGF1-induced suppression of lipolysis in 3T3-L1 adipocytes. Cells were pretreated with indicated doses of FGF1 for 10 min prior to the induction of lipolysis with 100 nM isoproterenol (ISO), and the cumulative release of FFAs over 4h measured. Data are represented as mean  $\pm$  SEM (n = 3, \*\* $p$  < 0.01, \*\*\* $p$  < 0.001).

- D) Serum FFA levels in overnight fasted adR1WT and adR1KO DIO mice 30 min after vehicle (PBS) or FGF1 (0.5 mg/kg) injection. Data are represented as mean  $\pm$  SEM (adR1WT vehicle n = 5, FGF1 n=5; adR1KO vehicle n = 4, FGF1 n=4 \* $p$  < 0.05).
- E) *Ex-vivo* lipolysis in gWAT explants from overnight fasted adR1WT and adR1KO DIO mice 2 h after vehicle (PBS) or FGF1 (0.5 mg/kg) injection. Data are represented as mean  $\pm$  SEM (n = 5 per group, \* $p$  < .05).
- F)  $^3\text{H}$ -labeled oleic acid turnover in chow-fed adR1WT and adR1KO mice. Overnight fasted mice were injected with vehicle (PBS) or FGF1 (0.5 mg/kg, s.c.) 6 hours prior to the portal vein infusion of  $^3\text{H}$ -labeled oleic acid. Plasma radioactivity was measured by scintillation counting and normalized to t=1 min. Fractional oleic acid turnover rate calculated by linear regression of natural log transformed data (adR1WT vehicle n = 5, FGF1 n = 4; adR1KO vehicle n = 4, FGF1 n = 5). Data are represented as mean  $\pm$  SEM (\*  $p$  < .05).
- G) *Ad lib* fed blood glucose levels in vehicle (PBS) and FGF1 injected (0.5 mg/kg) *ob/ob* mice with and without co-administration of the ATGL inhibitor atglistatin (120 mg/kg p.o) (Veh, n = 5; FGF1, n = 4; ATGLi, n = 5; ATGLi+FGF1, n = 6). Data are represented as mean  $\pm$  SEM. (\*  $p$  < 0.05).
- H) Western blots of total and S660 phosphorylated HSL (pHSL) in 3T3-L1 adipocytes 10 min after vehicle or FGF1 (100 ng/ml) treatment. Quantification of pHSL-S660 normalized to total HSL is shown in the right panel. Data are represented as mean  $\pm$  SEM (n = 4, \* $p$  < 0.05).
- I) Western blots of total and S660 phosphorylated HSL (pHSL) in gWAT from chow-fed C57BL/6J mice 30 min after vehicle (PBS), FGF1 (0.5 mg/kg) or insulin (1 U/kg) injection. Quantification of pHSL-S660 normalized to total HSL (right panel). (Veh, FGF1, n = 5; insulin, n = 4). Data are represented as mean  $\pm$  SEM (\*\* $p$  < 0.01, \*\*\* $p$  < 0.001). See also Figure S1.



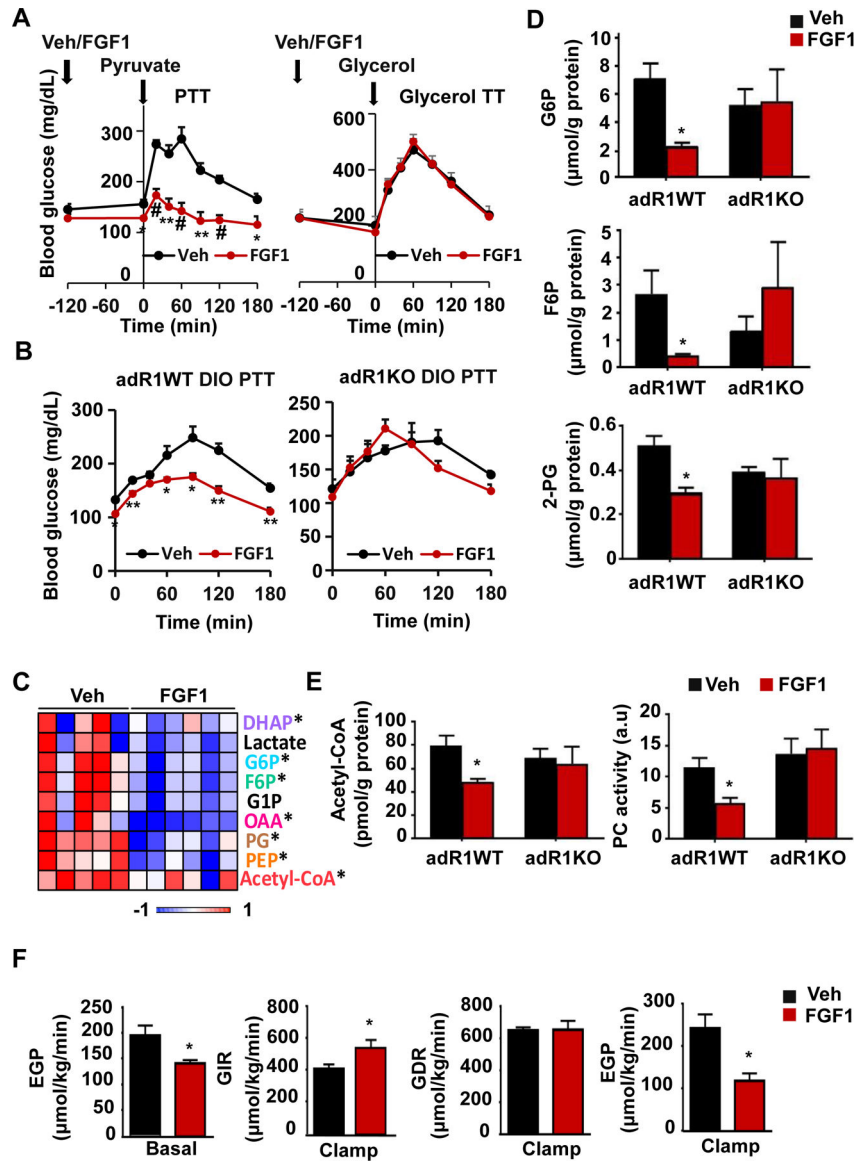


**Figure 2. FGF1 suppresses hepatic glucose production (HGP) in an adipose FGFR1 dependent manner**

A) Pyruvate tolerance test (PTT, left panel) and glycerol tolerance test (Glycerol TT, right panel) in overnight fasted *ob/ob* mice 2 h after vehicle (PBS) or FGF (0.5 mg/kg) injection. Data are represented as mean  $\pm$  SEM (n = 5 per group; \* $p$  < 0.05, \*\* $p$  < 0.01, # $p$  < 0.001).

B) PTTs in adR1WT and adR1KO DIO mice, as described in A. Data are represented as mean  $\pm$  SEM (n = 4 per group, \* $p$  < 0.05, \*\* $p$  < 0.01).

C) Heatmap of hepatic metabolites in *ob/ob* mice 2 h after vehicle (PBS) or FGF1 (0.5 mg/kg) injection. DHAP, dihydroxyacetone phosphate; G6P, glucose 6-phosphate; F6P, fructose 6-phosphate; G1P, glucose 1-phosphate; OAA, oxaloacetate; PG, phosphoglycerate; PEP, phosphoenolpyruvate. Vehicle n=5, FGF1 n=6, \* $p$  < 0.05.

D) Hepatic G6P, F6P and 2-phosphoglycerate (2-PG) levels in HFD-fed adR1WT and adR1KO mice 6 h after vehicle (PBS) or FGF1 (0.5 mg/kg) injection. adR1WT Veh n=8, FGF1=7; adR1KO veh n=6, FGF1=6. Data are represented as mean  $\pm$  SEM (\* $p$  < 0.05).

E) Hepatic acetyl-CoA levels (left panel) and pyruvate carboxylase (PC) activity (right panel) normalized by protein content in mice described in (D) (\* $p < 0.05$ ).

F) Basal and glucose-clamped levels of endogenous glucose production (EGP), glucose infusion rate (GIR), and glucose disposal rate (GDR) in *ob/ob* mice after one week of vehicle (PBS) or FGF1 (0.5 mg/kg q.o.d.) injections, measured during a hyperinsulinemic clamp. Vehicle n=9, FGF1 n=8. Data are represented as mean  $\pm$  SEM (\* $p < 0.05$ ). See also Figure S2.

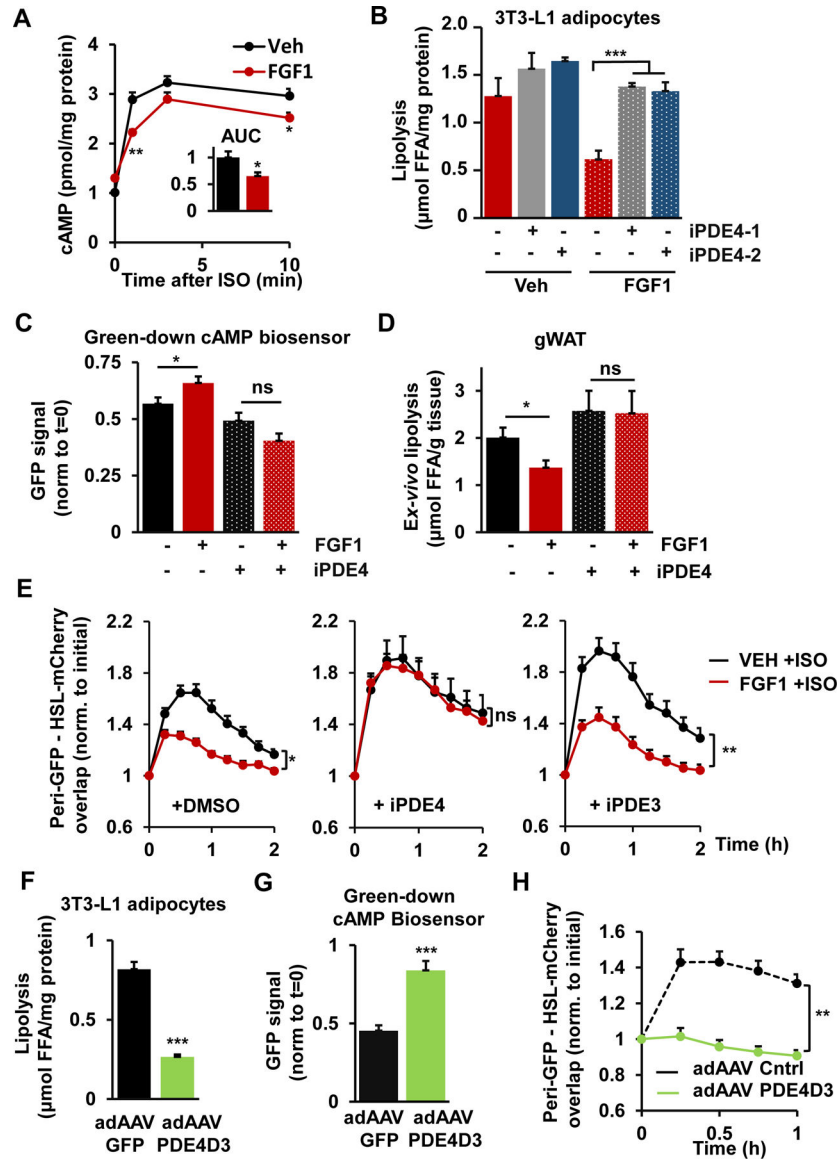


**Figure 3. FGF1 suppression of lipolysis is dependent on PDE4 activity**

A) Kinetics of isoproterenol (ISO, 100 nM) induced cAMP levels in 3T3-L1 adipocytes pretreated with vehicle (PBS) or FGF1 (100 ng/ml) for 15 min, as measured by ELISA. Data are represented as mean  $\pm$  SEM (n = 4, \* $p$  < 0.05, \*\* $p$  < 0.01).

B) 3T3-L1 adipocyte lipolysis after vehicle (PBS) or FGF1 (100 ng/ml) treatment in the presence or absence of PDE4 inhibitors (roflumilast, 2  $\mu$ M and cilomulast, 10  $\mu$ M). PBS or FGF1 was added 15 min prior to isoproterenol (100 nM) stimulation for 4 h. Data are represented as mean  $\pm$  SEM (n = 4, \*\*\* $p$  < 0.001).

C) cAMP levels in 3T3-L1 adipocytes, pretreated for 15 min with vehicle (PBS) or FGF1 (100 ng/ml) with or without PDE4 inhibitor (roflumilast, 2  $\mu$ M), 30 min after isoproterenol treatment (100 nM). Normalized GFP fluorescence from cAMP biosensor. Data are presented as mean  $\pm$  SEM (n = 12, \* $p$  < 0.05).

D) Lipolysis in gWAT explants from overnight-fasted DIO mice pretreated with the PDE4 inhibitor (roflumilast, 5 mg/kg p.o.) 1 h prior to vehicle (PBS) or FGF1 (0.5 mg/kg) injection. Mice were sacrificed 2 h later. Data are represented as mean  $\pm$  SEM (n = 6, \* $p$  < 0.05).

E) Kinetics of isoproterenol (ISO, 100 nM) induced perilipin-GFP and HSL-mCherry co-localization in 3T3-L1 adipocytes pretreated for 15 min with vehicle (PBS) or FGF1 (100 ng/ml). Effects of PDE4 (roflumilast, 2  $\mu$ M; middle panel) and PDE3 (cilostamide, 10  $\mu$ M; right panel) inhibitors on co-localization. Data are represented as mean  $\pm$  SEM (n = 12, \* $p$  < 0.05, \*\* $p$  < 0.01).

F) Lipolysis in 3T3-L1 adipocytes infected with an adipose specific AAV (adAAV) expressing GFP or PDE4D3. Data are represented as mean  $\pm$  SEM (n = 7, \*\*\* $p$  < 0.001).

G) cAMP levels in 3T3-L1 adipocytes infected with adAAVs expressing GFP or PDE4D3 30 min after isoproterenol treatment (100 nM), measured using the Green-down biosensor. Data are represented as mean  $\pm$  SEM (n = 14, \*\* $p$  < 0.01).

H) Kinetics of isoproterenol-induced perilipin-GFP and HSL-mCherry co-localization in 3T3-L1 adipocytes infected with adAAVs expressing PDE4D3 or control vector without an open reading frame. Data are represented as mean  $\pm$  SEM (n = 19, \*\* $p$  < 0.01). See also Figure S3.

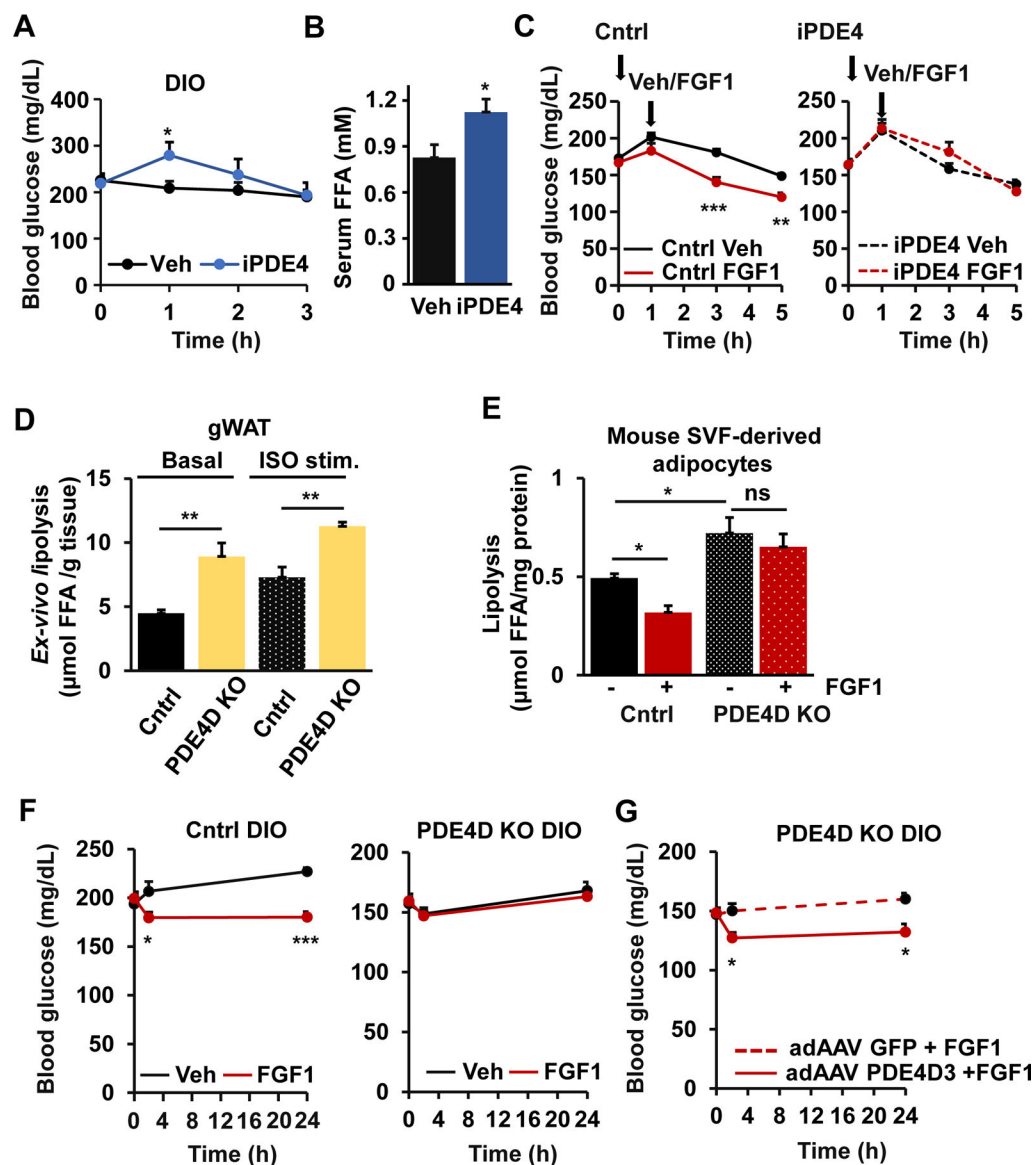


**Figure 4. FGF1-induced suppression of lipolysis and blood glucose in dependent on PDE4D**

A) Blood glucose levels in *ad lib* fed DIO mice after administration of vehicle (30 % captisol) or the PDE4 inhibitor roflumilast (5 mg/kg p.o.). Data are represented as mean  $\pm$  SEM (n = 5 per group, \*\*\* $p$  < 0.001).

B) Serum FFA levels 1 h after the injection of the vehicle or the PDE4 inhibitor in the mice described in (A).

C) *ad lib* fed blood glucose levels in DIO mice injected with vehicle (PBS) or FGF1 (0.5 mg/kg) in the absence (left panel) or presence (right panel) of the PDE4 inhibitor roflumilast (5 mg/kg). Mice were fasted after the 0 h time point. Data are represented as mean  $\pm$  SEM (Cntrl Veh n=7, Cntrl FGF1 n=6, iPDE4 Veh n=7, iPDE4 FGF1 n=8 per arm, \*\*  $p$  < 0.01, \*\*\* $p$  < 0.001).

D) Basal and isoproterenol-stimulated (ISO, 1  $\mu$ M) lipolysis in gWAT explants from overnight fasted, chow-fed control and PDE4D KO mice. Data are represented as mean  $\pm$  SEM (n = 4 per group, \*\* $p < 0.01$ ).

E) Isoproterenol-induced lipolysis (1 nM) in SVF-derived adipocytes from control and PDE4D KO mouse. Cells were pretreated with vehicle (PBS) or FGF1 (100 ng/ml) for 10 min prior to Isoproterenol addition. Data are represented as mean  $\pm$  SEM (n = 4 per treatment, \* $p < 0.05$ ).

F) *ad lib* fed blood glucose levels in control and PDE4D KO DIO mice after vehicle (PBS) or FGF1 (0.5 mg/kg) injection. Mice were fasted after the injection until the 2 h time point, then food was returned. Data are represented as mean  $\pm$  SEM (n = 6 per group, \* $p < 0.05$ , \*\*\* $p < 0.001$ ).

G) *ad lib* fed blood glucose levels after FGF1 injection (0.5 mg/kg) in PDE4D KO DIO mice 4 weeks after treatment with adAAVs driving the expression of PDE4D3 or GFP. Data are represented as mean  $\pm$  SEM (n = 7 per group, \* $p < 0.05$ ). See also Figure S4.

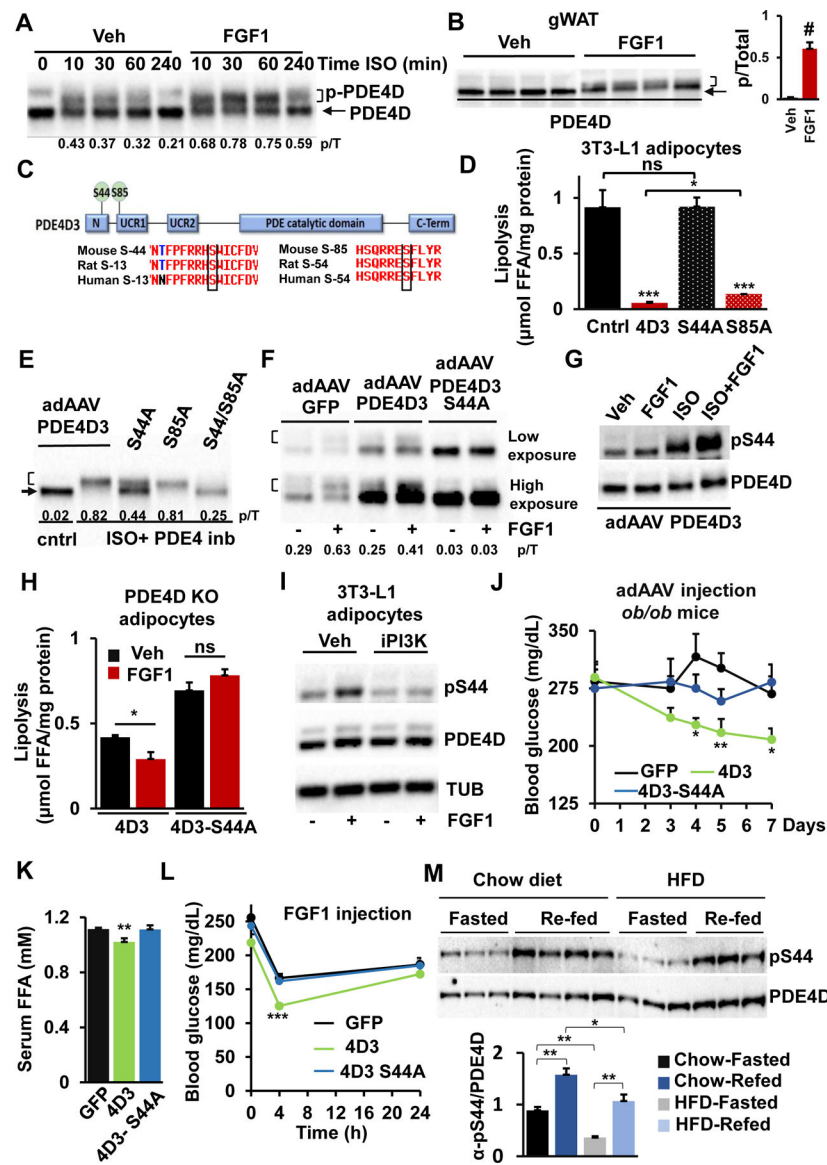


**Figure 5. PDE4D3-S44 phosphorylation is required for the metabolic effects of PDE4D3**

A) Representative Western blot among three independent experiments showing the temporal changes in isoproterenol-induced PDE4D phosphorylation in 3T3-L1 adipocytes pretreated for 15 min with vehicle (PBS) or FGF1 (100 ng/ml). Bracket indicates the phosphorylated, slower migrating PDE4D fraction whereas arrow shows the hypo-phosphorylated form. Quantification of the phospho-band to total is shown below.

B) Western blots of PDE4D phosphorylation in gWAT from overnight-fasted chow-fed C57BL/6J mice 30 min after vehicle (PBS) or FGF1 (0.5 mg/kg) injection. Quantification of the phospho-band to total is shown on the right. Data are represented as mean  $\pm$  SEM (n = 4/arm, #p < 0.001).

C) Scheme of mouse PDE4D3 domains and known PKA phosphorylation sites. The conservation of phosphorylation sites between mouse, rat, and human PDE4D3 is shown below.

D) Lipolysis in 3T3-L1 adipocytes infected with adAAVs expressing GFP (control), PDE4D3 (4D3), PDE4D3 S44A, or PDE4D3 S85A. Data are represented as mean  $\pm$  SEM (n = 3 per treatment group, \*\*\* $p$  < 0.001).

E) Representative Western blot from two-independent experiments showing PDE4D3 expression in 3T3-L1 adipocytes infected with adAAVs expressing wildtype, S44A, S85A, or S44A/S85A PDE4D3 30 min after treatment with isoproterenol (1  $\mu$ M) and the PDE4 inhibitor roflumilast (4  $\mu$ M). Arrow indicates hypo-phosphorylated, bracket indicates phosphorylated PDE4D3. Quantification of the phospho-band to total is shown below.

F) Representative Western blot from three independent experiments showing PDE4D3 levels after 30min isoproterenol treatment of (100 nM) 3T3-L1 adipocytes infected with adAAVs expressing GFP, wildtype PDE4D3 or PDE4D3 S44A with or without 15 min FGF1 pre-treatment (100 ng/ml) (low exposure-upper panel, high exposure-lower panel). Brackets indicates phosphorylated PDE4D3. Quantification of the phospho-band to total is shown below.

G) Western blots of S44 phosphorylated (upper panel) and total PDE4D (lower panel) in 3T3-L1 adipocytes infected with adAAV PDE4D3 after indicated treatments (FGF1, 10 min pretreatment at 100 ng/ml; ISO, 100 nM isoproterenol for 30 min; or FGF1 pre-treatment and 30 min ISO treatment. Quantification of pS44/Total PDE4D is shown in S5E.

H) Isoproterenol-induced (1 nM) lipolysis in SVF-derived adipocytes from PDE4D KO mouse infected with adAAVs expressing WT or S44A PDE4D3 pretreated with vehicle (PBS) of FGF1 (100 ng/ml) for 10 min. Data are represented as mean  $\pm$  SEM (n = 4 per treatment, \* $p$  < 0.05).

I) Western blots showing PDE4D-S44 phosphorylation in 3T3-L1 adipocytes 15 min after vehicle (PBS) or FGF1 (100 ng/ml) treatment. Cells were pretreated with the PI3K inhibitor wortmannin (5 $\mu$ M) or DMSO 30 min before Veh or FGF1 treatment. Quantification of pS44/total PDE4D is shown in S5H.

J) *ad lib* fed blood glucose levels in *ob/ob* mice injected with adAAVs expressing GFP (n=9), PDE4D3 (n=8) or PDE4D3 S44A (n = 8). Data are represented as mean  $\pm$  SEM (\* $p$  < 0.05, \*\* $p$  < 0.01)

K) *ad lib* fed serum free fatty acid levels of *ob/ob* mice described in (J). Data are represented as mean  $\pm$  SEM (n = 8 per arm; \*\* $p$  < 0.01).

L) *ad lib* fed blood glucose levels of the mice described in (J) after FGF1 (0.5 mg/kg) injection. Mice were fasted after the injection until the 4 h time point, then food was returned. Data are represented as mean  $\pm$  SEM (adAAV GFP and adAAV PDE4D3, n = 7; adAAV PDE4D3 S44A, n = 5; \*\*\* $p$  < 0.001).

M) Western blots of S44 phosphorylated (upper panel) and total (lower panel) PDE4D in overnight-fasted and 4 h refeed mice maintained on chow and HFD. Quantification of pS44 levels normalized to total PDE4D levels. Data are represented as mean  $\pm$  SEM (\* $p$  < 0.05, \*\* $p$  < 0.01). See also Figure S5.



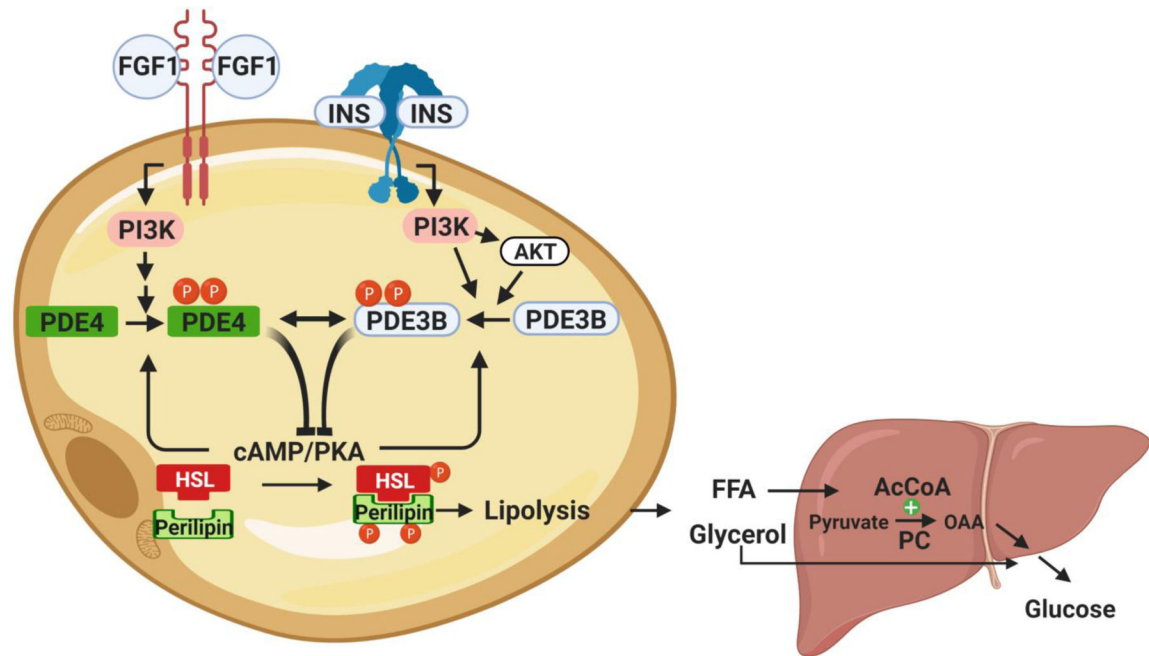


**Figure 6. Model of FGF1-induced suppression of lipolysis and HGP**

Distinct FGF1 signaling parallels insulin-induced suppression of adipose lipolysis and hepatic glucose production (HGP). FGF1/FGFR1 signaling in adipocytes activates PDE4 to decrease cAMP levels and thereby PKA activity. Reduced PKA activity attenuates HSL phosphorylation/translocation to suppress lipolysis. FGF1-induced suppression of lipolysis reduces hepatic glucose production (HGP) through the allosteric regulation of pyruvate carboxylase.

## KEY RESOURCES TABLE

| REAGENT or RESOURCE                                      | SOURCE                               | IDENTIFIER                  |
|--|--------------------------------------|-----------------------------|
| <b>Antibodies</b>  |                                      |                             |
| PDE4D  | Proteintech                          | 12918-1-AP, RRID:AB_2161097 |
| pHSL   | Cell Signaling                       | 4126S, RRID:AB_490997       |
| HSL  | Cell Signaling                       | 4107S, RRID:AB_2296900      |
| GFP  | GenScript                            | A01388, RRID:AB_1720867     |
| $\alpha$ -Tubulin  | Millipore Sigma                      | CP06, RRID:AB_2617116       |
| PDE4D-pS44   | This paper                           | RRID:AB_2894884             |
| <b>Bacterial and Virus Strains</b>                       |                                      |                             |
| AAV2/8-phadipoq-GFP- miRNA122T <sub>4x</sub>             | This paper                           | adAAV-GFP                   |
| AAV2/8-phadipoq-PDE4D3- miRNA122T <sub>4x</sub>          | This paper                           | adAAV-PDE4D                 |
| AAV2/8-phadipoq-PDE4D3-S44A-miRNA122T <sub>4x</sub>      | This paper                           | adAAV-PDE4D-S44A            |
| AAV2/8-phadipoq-PDE4D3-S85A-miRNA122T <sub>4x</sub>      | This paper                           | adAAV-PDE4D-S85A            |
| AAV2/8-phadipoq-PDE4D3-S44A-S85A-miRNA122T <sub>4x</sub> | This paper                           | adAAV-PDE4D-S44A-S85A       |
| Ad5-CMV-PDE4D3   | This paper                           | Ad5-4D3                     |
| Ad5-CMV-PDE4D4   | This paper                           | Ad5-4D4                     |
| Ad5-CMV-PDE4D5   | This paper                           | Ad5-4D5                     |
| AAV2/8-phadipoq-mCherry- miRNA122T <sub>4x</sub>         | This paper                           | adAAV-mCherry               |
| AAV2/8-phadipoq-HSL-mCherry- miRNA122T <sub>4x</sub>     | This paper                           | adAAV-HSL-mCherry           |
| AAV2/8-phadipoq-Perilipin-GFP- miRNA122T <sub>4x</sub>   | This paper                           | adAAV-Perilipin-GFP         |
| Green Down cADDIS cAMP Sensor BacMam                     | Montana Molecular                    | D0200G                      |
| mNeon Green Control BacMam                               | Montana Molecular                    | F0505G                      |
| OneShot Stbl3 Ecoli                                      | Invitrogen                           | C737303                     |
| <b>Chemicals, Peptides, and Recombinant Proteins</b>     |                                      |                             |
| Roflumilast  | Tocris Bioscience                    | 6641/50                     |
| Cilomulast   | Santa Cruz                           | sc-483188                   |
| Cilostamide  | Cayman Chemicals                     | 14455-25                    |
| Quazinine  | Enzo Life Sciences                   | BML-PD170-0010              |
| Isoproterenol hydrochloride                              | Tocris Biosciences                   | 1747/100                    |
| Captisol   | Selleckchem                          | S4592                       |
| dexamethasone  | Sigma-Aldrich                        | D1756                       |
| rosiglitazone  | Sigma-Aldrich                        | R2408                       |
| IBMX   | Cayman Chemicals                     | 13347-500                   |
| fatty acid free BSA                                      | United States Biological Corporation | A1311250G                   |
| [U-13C] glucose  | Cambridge Isotop Lab.                | CLM-1396-PK                 |
| Recombinant FGF1   | Exonbio                              | N/A                         |
| Collagenase I  | Worthington                          | LS004196                    |

| REAGENT or RESOURCE   | SOURCE                   | IDENTIFIER             |
|---|--------------------------|------------------------|
| Insulin (for <i>in vivo</i> injection)  | MED-VET INTL             | RXHUMULIN-R            |
| Insulin (for cell-based studies)  | Sigma                    | I1882                  |
| insulin (used for clamp study)  | Novo Nordisk             | N/A                    |
| somatostatin  | UCB Breda                | N/A                    |
| 5'-Nucleotidase   | Enzo Life Sciences       | BML-K1307              |
| [3H]-cAMP   | Perkin Elmer             | NET275250UC            |
| $\alpha$ -PDE4D3-S44 antigen: FRRHpSWISFDVDNGTSAGRC                             | RS Synthesis             | N/A                    |
| <b>Critical Commercial Assays</b>   |                          |                        |
| FFA kit   | Wako                     | NEFAHR2                |
| ViraPower™ Adenoviral Gateway™ Expression Kit                                   | Thermo Fisher Scientific | K493000                |
| Adenovirus standard purification kit  | Virapur                  | 3054                   |
| Hi Pure Purelink Expi Plasmid Giga Prep   | Thermo Fisher Scientific | K210009XP              |
| QuickChange XL Site-Directed Mutagenesis Kit                                    | Agilent                  | 200517                 |
| Deproteinization Assay Kit  | BioVision                | K808200                |
| 2-Phosphoglycerate Colorimetric/Fluorometric Assay Kit                          | BioVision                | K778                   |
| PicoProbe Acetyl CoA Assay Kit  | BioVision                | K317                   |
| PicoProbe Fructose-6-Phosphate Fluorometric Assay Kit                           | BioVision                | K689                   |
| PicoProbe Glucose-6-Phosphate Fluorometric Assay Kit                            | BioVision                | K687                   |
| Thermo Scientific™ Maxima H Minus First Strand cDNA Synthesis Kit, with dsDNase | Thermo Fisher Scientific | K1681                  |
| <b>Deposited Data</b>   |                          |                        |
| Targeted metabolite measurements in liver                                       | This paper               | MSV000088351           |
| <b>Experimental Models: Cell Lines</b>  |                          |                        |
| 3T3-L1 cells  | ATCC                     | CL-173, RRID:CVCL_0123 |
| Human subcutaneous pre-adipocytes   | Promocell                | C-12735                |
| <b>Experimental Models: Organisms/Strains</b>                                   |                          |                        |
| C57BL/6J  | JAX                      | 000664                 |
| B6.Cg-Lepob/J   | JAX                      | 000632                 |
| B6;FVB-Tg(Adipoq-cre)1Evdr/J  | JAX                      | 010803                 |
| B6.129S4-Fgfr1tm5.1Sor/J  | JAX                      | 00767                  |
| B6N.129P2-Pde4dtm1Mct/Mmucd   | MMRRC                    | 034588-UCD             |
| <b>Oligonucleotides</b>   |                          |                        |
| See Table S2 for oligonucleotides used in the study                             |                          |                        |
| <b>Recombinant DNA</b>  |                          |                        |
| Plin1 (GFP-tagged) ORF clone  | Origene                  | MG222553               |
| AAV2-phadipoq-miRNA122T <sub>4x</sub>   | This paper               | N/A                    |
| AAV2-phadipoq-GFP- miRNA122T <sub>4x</sub>                                      | This paper               | N/A                    |
| AAV2-phadipoq-PDE4D3- miRNA122T <sub>4x</sub>                                   | This paper               | N/A                    |
| AAV2-phadipoq-PDE4D3-S44A-miRNA122T <sub>4x</sub>                               | This paper               | N/A                    |

| REAGENT or RESOURCE                                    | SOURCE     | IDENTIFIER |
|--|------------|------------|
| AAV2-phadipoq-PDE4D3-S85A-miRNA122T <sub>4x</sub>      | This paper | N/A        |
| AAV2-phadipoq-PDE4D3-S44A-S85A-miRNA122T <sub>4x</sub> | This paper | N/A        |
| Ad5-CMV-PDE4D3   | This paper | N/A        |
| Ad5-CMV-PDE4D4   | This paper | N/A        |
| Ad5-CMV-PDE4D5   | This paper | N/A        |
| AAV2-phadipoq-mCherry- miRNA122T <sub>4x</sub>         | This paper | N/A        |
| AAV2-phadipoq-HSL-mCherry-miRNA122T <sub>4x</sub>      | This paper | N/A        |
| AAV2-phadipoq-Perilipin-GFP-miRNA122T <sub>4x</sub>    | This paper | N/A        |

Author Manuscript

Author Manuscript

Author Manuscript

Author Manuscript